IEEE Access
Multidisciplinary | Rapid Review | Open Access Journal

SPECIAL SECTION ON ADVANCES IN POWER LINE COMMUNICATION AND ITS APPLICATIONS

Received June 3, 2019, accepted June 16, 2019, date of publication July 3, 2019, date of current version August 6, 2019.

Digital Object Identifier 10.1109/ACCESS.2019.2926750

Performance Analysis of Two-Way Relaying in Cooperative Power Line Communications

ROGER KWAO AHIADORMEY, (Student Member, IEEE), PRINCE ANOKYE, (Member, IEEE), HAN-SHIN JO, (Member, IEEE), AND KYOUNG-JAE LEE, (Member, IEEE)

Department of Electronics and Control Engineering, Hanbat National University, Daejeon 34158, South Korea

Corresponding author: Kyoung-Jae Lee (kyoungjae@hanbat.ac.kr)

This work was supported in part by the Korea Electric Power Corporation under Grant R17XA05-71, and in part by the Institute for Information and Communications Technology Promotion (IITP) Grant funded by the Korea Government (MIST) under Grant 2016-0-00500 (Cross layer design of cryptography and physical layer security for IoT networks).

ABSTRACT This paper studies the performance of a half-duplex (HD) two-way relay (TWR) in power line communication (PLC) over a log-normal fading channel with impulsive noise. We consider the two common relaying protocols: amplify-and-forward (AF) and decode-and-forward (DF). For the DF relaying, we apply physical-layer network coding (PNC) and analog-network coding (ANC) to the PLC TWR. We derive analytic expressions for the average sum capacity and the outage probability of the system. The Monte Carlo simulations are provided throughout to validate our analysis. The analytical results show a tight approximation to the simulation results. We compare the one-way relay (OWR) to the TWR and show that the HD spectral efficiency loss incurred by the OWR can be sufficiently mitigated in PLC. However, the outage probability of the TWR is inferior to that of the OWR. To enhance the outage performance of the PLC TWR, we implement a hybrid PLC/wireless (HPW) system, where all nodes are equipped with the PLC and wireless capabilities. Data transmission occurs over the two parallel links. The diversity in the transmission allows the TWR to improve its outage performance in the AF and DF protocols. The impact of the impulsive noise, inherent to the PLC channels, is also highlighted in the simulation results. It is shown that the impulsive noise severely impairs system performance.

INDEX TERMS Two-way relaying, average capacity, outage probability, power line communication (PLC), PLC/wireless diversity.

I. INTRODUCTION

Smart grid (SG) technology is considered an integral part of next-generation electric power grids to improve upon the quality of service (QoS). SGs allow a bidirectional exchange of data that gives utilities the ability to provide a wide range of essential services such as smart metering, load management, data privacy, and security [1]. Although there are several candidates for communication in the SG, power line communication (PLC) has gained a preeminent spotlight since it uses the existing power lines [1]. Thus, there is no need to build new infrastructure. To transmit a data signal in PLC, a coupling circuit injects a modulated carrier signal onto the power line. At the receiving end, another coupler is utilized to separate the transmitted data signal and decoding ensues. Depending on the operating frequency, PLC technology can be broadly grouped as narrowband (NB) or broadband (BB) [2]. NB PLC typically operates in the 3-500kHz range and is accompanied by low data rates. NB PLC is appropriate for smart metering, smart homes, monitoring, and control applications [2]. To meet the high data demands in multimedia services, BB PLC which operates in the 1.8-250MHz range offers high data rates and typically employed in in-home applications (e.g., high-speed internet access) [2]. In view of this, several PLC standards have been proposed for SG applications [3]–[5].

However, the data rates and the reliability of the PLC network are affected by increased impulsive noise, interference, multipath effects, and signal fading over long cable lengths. To overcome these challenges, multiple-input multiple-output (MIMO), orthogonal frequency division multiplexing (OFDM), non-orthogonal multiple access (NOMA), and relaying have been proposed for the PLC network [6]–[9]. In [6], by combining MIMO and

The associate editor coordinating the review of this manuscript and approving it for publication was Khaled Rabie.

OFDM with a power allocation algorithm, precoded spatial multiplexing increases the PLC channel capacity and link reliability for different levels of quantized channel state information (CSI). Compared to conventional PLC systems that utilize orthogonal multiple access (OMA) schemes, NOMA PLC has been recently proposed for DF cooperative PLC networks to increase the system capacity, reduce electromagnetic emissions, and improve the fairness between different users [7].

With hybrid PLC/wireless (HPW) diversity, PLC nodes are equipped with additional wireless capabilities to offer performance enhancements [10], [11]. Results show an HPW system guarantees reliable transmission even when the link quality of either medium deteriorates. Owing to its versatility, the application of other PLC performance-enhancing techniques to HPW systems follows directly. The achievable rate performance of an HPW energy harvesting relay is analyzed in [12]. The physical layer security issue in OFDM based HPW is highlighted in [13], where artificial noise is used to compromise eavesdropper attacks. The design of a dual-interface relay for HPW applications is the main focus of [14]. Here, the relay selects an interface (PLC or wireless) according to the CSI to enhance system performance in terms of the bit-error rate (BER), average capacity, and outage probability.

In cooperative networks, relaying is shown to increase link reliability and extend coverage, especially when there is no direct link between a transmitting node and a receiving node [15]. Compared to a one-way relay (OWR), a two-way relay (TWR) has the potential to increase the spectrum efficiency (SE) as duplex communication can be achieved in two time slots by employing physical-layer network coding (PNC) or analog network coding (ANC) at the relay [16]–[22]. Considering the data exchange in the SG, next-generation electric power grids with two-way communications are expected to increase the data rate, system reliability, and security [23]. The two common relaying protocols are the amplify-and-forward (AF) and the decode-and-forward (DF) protocols. An AF relay simply amplifies the received signal and retransmits, whereas the DF relay decodes the received signal before retransmission to the destination. Comparing the two protocols, the AF relay suffers from noise amplification, while the DF relay has a higher processing cost [24]–[28].

In PLC, the AF and DF protocols for the OWR have been studied to a great extent. More specifically in [8], the authors analyzed the performance of cooperative schemes for a dual-hop single relay based on in-home PLC channel measurements. The achievable rates for the AF and the DF protocols are derived for different diversity combining techniques. It is shown that the DF protocol can improve the performance of in-home PLC networks compared to the AF protocol. To improve the energy efficiency of cooperative PLC, the outage probability of an AF and a DF OWR with energy harvesting is derived in [29] and [30], respectively. The work in [31] presents an analog full-duplex AF relay, where optimizing the analog circuit parameters leads to an increase in the communication rate. The authors of [32] analyzed multihop DF relaying to include the effects of Rayleigh fading and Bernoulli-Laplacian noise in PLC networks. The spectral efficiency and outage probability of incremental relaying in PLC networks are significantly improved by optimizing relay usage and power allocation in [33].

Considering the inherent spectral efficiency loss associated with OWR, it is imperative to study the performance of TWRs in PLC. However, few works have studied the TWR in PLC systems [34]–[37]. Performance analysis of an AF TWR in PLC is carried out in [34], where the authors derived closed-form expressions for the outage probability, the symbol error rate, and the average capacity. However, the DF relaying protocol and the effect of PLC channel attenuation are not accounted for. The authors of [35] studied the capacity performance of an OWR and a TWR by considering both AF and DF schemes in a bottom-up channel model. Here, the DF protocol is shown to provide more robust performance in terms of SE. Relay power optimization for an AF TWR in an indoor broadband PLC setting is investigated in [36]. The proposed alternating optimization algorithm reduces the power consumption associated with a TWR. In [37], the authors presented a PLC network with PNC to boost the capacity of TWRs. However, performance analysis of the protocols was not considered in [36] and [37].

Motivated by this, we analyze the performance of a half-duplex PLC TWR for both relaying protocols and networking coding schemes in realistic channel environments, and we further propose a technical solution leveraging channel diversity. Based on the result that the PLC channel characteristics can be approximated by log-normal fading, we consider the PLC channel with log-normal distribution [38]–[40]. The power line induced noise is modeled as a combination of background and impulsive noise [41]. Moreover, unlike the work in [34], we account for the distance-dependent signal attenuation. We analyze the average sum capacity and the outage probability of an AF and a DF TWR in PLC. In particular, for the DF protocol, we apply the two network coding schemes, ANC and PNC to increase the average sum capacity. The derived analytic expressions are shown to be tight in comparison with Monte Carlo simulations. Since the PLC channel suffers from impulsive noise, its impact is accounted for in the analysis. The results show that higher impulsive noise probability leads to lower average capacity and a higher outage probability across all protocols. In addition, a comparison is performed to ascertain the gain of the PLC TWR over the PLC OWR. The numerical results also reveal that the outage probability of the DF protocol is severely limited by the decoding strategy at the relay. Based on the analytic results, we propose an HPW diversity technique where all nodes are equipped with PLC and wireless capabilities to enhance the reliability of the TWR. Data transmission occurs over the two parallel links where the wireless link is modeled as a Rayleigh fading channel. Compared to a single transmission medium (i.e., PLC only or wireless only),

TABLE 1. Summary of abbreviations.

Acronym	Definition
AF	Amplify-and-Forward
ANC	Analog Network Coding
BC	Broadcast
CCDF	Complementary Cumulative Distribution Function
CDF	Cumulative Distribution Function
DF	Decode-and-Forward
HD	Half-Duplex
HPW	Hybrid PLC/Wireless
MAC	Mutiple Access
MGF	Moment Generating Function
OWR	One-Way Relay
PDF	Probability Density Function
PLC	Power Line Communication
PNC	Physical-layer Network Coding
SI	Self-Interference
SIC	Successive Interference Cancellation
SINR	Signal-to-Impulsive Noise Ratio
SNR	Signal-to-background Noise Ratio
TDD	Time Division Duplex
TWR	Two-Way Relay

the HPW system performs better in terms of the outage probability.

The rest of the paper is organized as follows: Section II describes the system model for the PLC TWR network. Analytic expressions for the average sum capacity and the outage probability for the AF and DF protocols are derived in Section III. In Section IV, we propose a hybrid PLC/wireless system and analyze the outage probability for the AF and the DF TWR. The simulation results are discussed in Section V. Conclusions follow in Section VI.

Notation: $f_X(\cdot)$, $F_X(\cdot)$, and $\bar{F}_X(\cdot)$ denote the probability density function (PDF), the cumulative distribution function (CDF), and the complementary CDF (CCDF) of the random variable (RV) X, respectively. $F_X(\cdot)$ and $\bar{F}_X(\cdot)$ are related by $\bar{F}_X(\cdot) = 1 - F_X(\cdot)$. $\mathcal{M}_X(\cdot)$, $\mathbb{E}[\cdot]$, $\Pr(\cdot)$, $Q(\cdot)$, and $\min(\cdot)$ denote the moment generating function (MGF) of a RV X, the expectation, the probability, the Q function, and the minimum operators, respectively. Some of the major abbreviations used in this paper are predefined in Table 1.

II. SYSTEM MODEL

Consider a three-node TWR system model which consists of two source nodes and a relay node as illustrated in Fig. 1. The source nodes $\mathcal{A}$ and $\mathcal{B}$ transmit their data to each other through the intermediate relay $\mathcal{R}$ due to the absence of a direct link. All nodes operate in the half-duplex mode. Data transmission occurs in two phases, i.e., the multiple access (MAC) phase and the broadcast (BC) phase. In the MAC phase, the source nodes $\mathcal{A}$ and $\mathcal{B}$ transmit their data to the relay $\mathcal{R}$ simultaneously. After receiving the transmitted data,

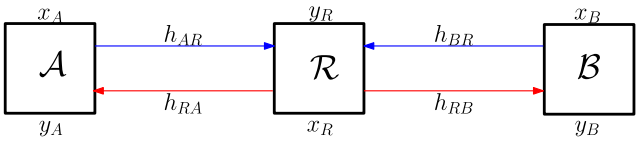

FIGURE 1. System model of a half-duplex PLC TWR.

the relay employs the AF or DF protocol with PNC (or ANC). In the BC phase, the relay retransmits the received data to the destination nodes $\mathcal{A}$ and $\mathcal{B}$. Since nodes $\mathcal{A}$ and $\mathcal{B}$ know their own transmitted signals, they can subtract the back-propagating self-interference (SI) signal before decoding.

The node $\mathcal{A}$ to relay, node $\mathcal{B}$ to relay, relay to node $\mathcal{A}$, and relay to node $\mathcal{B}$ channel coefficients are denoted as h_{AR}, h_{BR}, h_{RA}, and h_{RB}, respectively. We assume that the MAC channels and BC channels are reciprocal in a time division duplex (TDD) protocol [42][1]. It is also assumed that the CSI is perfectly known at the destination nodes for SI cancellation in the BC phase [46]. The amplitude of the channel coefficient h_i, $\forall i \in \{AR, BR, RA, RB\}$ is subjected to the log-normal distribution with PDF

$$f_{h_i}(z) = \frac{\xi}{\sqrt{2\pi}\sigma_i z} \exp\left[-\frac{(10\log_{10}(z) - \mu_i)^2}{2\sigma_i^2}\right], \quad z > 0, \tag{1}$$

where $\xi = 10/\ln(10)$ is a scaling constant, μ_i, and σ_i (both in decibels) are the mean and standard deviation of $10\log_{10} h_i$, respectively [30]. To account for the signal attenuation, we introduce a distance-dependent cable attenuation which is modeled by $a_i = \exp(-(b_0 + b_1 f^k)d_i)$, where d_i is the distance between the nodes, f represents the operating frequency in MHz, k is the exponent of the attenuation factor, b_0, and b_1 are the attenuation constants obtained from measurements [47].

In practical PLC networks, the channel is affected by a combination of background and impulsive noise. In decoding the received signal, all noise samples have to be considered. In this paper, we adopt the Bernoulli-Gaussian random process model which captures the combined effect of the background noise and the impulsive noise. Considering the independence of the background noise and impulsive noise, the total noise sample for any node has a PDF that is written as [48]

$$f_n(n) = (1-p)\mathcal{N}(n, 0, \sigma_G^2) + p\mathcal{N}(n, 0, \sigma_G^2 + \sigma_I^2), \tag{2}$$

where $\mathcal{N}(n, 0, \sigma_G^2)$ represents a Gaussian PDF of a RV n with mean zero and variance σ_G^2, $\mathcal{N}(n, 0, \sigma_G^2 + \sigma_I^2)$ represents a Gaussian PDF of a RV n with mean zero and variance $\sigma_G^2 + \sigma_I^2$, and p is the impulsive noise parameter that determines its

[1] In TWRs, the channels are estimated through various training based designs namely linear minimum mean square error estimation (LMMSE), maximum likelihood (ML) estimation, and Bayesian estimation [43]–[45]. With perfect synchronization between nodes, pilot sequences are transmitted and the transmit CSI can be acquired by assuming channel reciprocity in TDD operation.

probability of occurrence. The variances σ_G^2 and σ_I^2 denote the input signal-to-background noise ratio (SNR) and the signal-to-impulsive noise ratio (SINR), respectively.

In the MAC phase, both nodes $\mathcal{A}$ and $\mathcal{B}$ transmit their own signals to the relay simultaneously. Let P_A, P_B, and P_R denote the transmit powers of node $\mathcal{A}$, node $\mathcal{B}$, and the relay $\mathcal{R}$, respectively. The received signal at the relay is expressed as

$$y_R = \sqrt{P_A} a_{AR} h_{AR} x_A + \sqrt{P_B} a_{BR} h_{BR} x_B + n_R, \tag{3}$$

where x_A and x_B are the messages of node $\mathcal{A}$ and node $\mathcal{B}$, respectively, with $\mathbb{E}[|x_A|^2] = \mathbb{E}[|x_B|^2] = 1$. Also, n_R is the noise at the relay with zero mean and variance σ_R^2.

In the BC phase, the relay retransmits to nodes $\mathcal{A}$ and $\mathcal{B}$ after applying the AF or DF protocol. Finally, the signals received at the two nodes $\mathcal{A}$ and $\mathcal{B}$, are respectively, given by

$$y_A = a_{RA} h_{RA} x_R + n_A, \tag{4}$$

and

$$y_B = a_{RB} h_{RB} x_R + n_B, \tag{5}$$

where x_R is the transmitted signal of the relay. n_A and n_B denote the noise components at nodes $\mathcal{A}$ and $\mathcal{B}$ with zero mean and variances σ_A^2 and σ_B^2, respectively. In the next subsections, we look at the signal processing at the relay with the AF and the DF relaying strategies.

A. AMPLIFY-AND-FORWARD RELAYING

In the MAC phase, the relay receives the transmitted signals from the source nodes $\mathcal{A}$ and $\mathcal{B}$, amplifies the received signals and then retransmits to the nodes $\mathcal{A}$ and $\mathcal{B}$. At the destination nodes, since the nodes $\mathcal{A}$ and $\mathcal{B}$ know their own transmitted signals, they can perfectly subtract the back-propagating SI signal from the received signals before decoding. In the BC phase, by employing the AF protocol, the relay transmits the signal $x_R = \beta y_R$, where β is the constant relay gain defined as [35], [49][2]

$$\beta = \sqrt{\frac{P_R}{(P_A \mathbb{E}[a_{AR}^2 h_{AR}^2] + P_B \mathbb{E}[a_{BR}^2 h_{BR}^2] + \sigma_R^2)}}. \tag{6}$$

If γ_{A_0} represents the instantaneous SNR under only background noise and γ_{A_1} represents the instantaneous SNR under both background and impulsive noises, the resulting instantaneous SNRs of the AF TWR at nodes $\mathcal{A}$ and $\mathcal{B}$ are, respectively, written as

$$\gamma_{A_j} = \frac{P_B \beta^2 a_{BR}^2 a_{RA}^2 h_{RA}^2 h_{BR}^2}{\beta^2 a_{RA}^2 h_{RA}^2 \sigma_{R_j}^2 + \sigma_{A_j}^2}, \quad \forall j \in (0, 1), \tag{7}$$

and

$$\gamma_{B_j} = \frac{P_A \beta^2 a_{AR}^2 a_{RB}^2 h_{AR}^2 h_{RB}^2}{\beta^2 a_{RB}^2 h_{RB}^2 \sigma_{R_j}^2 + \sigma_{B_j}^2}, \quad \forall j \in (0, 1). \tag{8}$$

[2]In [50], the performance of fixed gain AF relays is comparable to the more complex variable gain AF relays. In this paper, we consider a fixed relay gain for simplicity.

B. DECODE-AND-FORWARD RELAYING

Here, we consider the network coding schemes, i.e., PNC and ANC. We consider an ideal case where the relay successfully decodes the received signals in the MAC phase [16]. With PNC, the relay applies a linear combination usually a bit-level exclusive OR (XOR) operation to the two received symbols to generate a new symbol [18]. The network coded symbol is transmitted to the nodes $\mathcal{A}$ and $\mathcal{B}$. In other words, after the relay decodes the signals received from the source nodes $\mathcal{A}$ and $\mathcal{B}$, it implements PNC and forwards the XOR-based re-encoded data to nodes $\mathcal{A}$ and $\mathcal{B}$ (now destination nodes). The signal transmitted by the relay in the BC phase is expressed as

$$x_R = \sqrt{P_R} x_C, \tag{9}$$

where $x_C = x_A \oplus x_B$ and $\oplus$ is the XOR operator. After decoding x_C from the received signals, the nodes $\mathcal{A}$ and $\mathcal{B}$ can perform the XOR operation of x_C with x_A and x_B, respectively, to obtain the desired signals, i.e., $x_B = x_C \oplus x_A$ for the node $\mathcal{A}$ and $x_A = x_C \oplus x_B$ for the node $\mathcal{B}$. The instantaneous SNR of the signals received at the relay $\mathcal{R}$, nodes $\mathcal{A}$, and $\mathcal{B}$ for both the MAC and BC phases are written as [18], [51], [52]

$$\gamma_{R_j} = \gamma_{AR_j} + \gamma_{BR_j}, \tag{10}$$

$$\gamma_{AR_j} = \frac{P_A a_{AR}^2 h_{AR}^2}{\sigma_{R_j}^2}, \quad \gamma_{BR_j} = \frac{P_B a_{BR}^2 h_{BR}^2}{\sigma_{R_j}^2}, \tag{11}$$

and

$$\gamma_{RA_j} = \frac{P_R a_{RA}^2 h_{RA}^2}{\sigma_{A_j}^2}, \quad \gamma_{RB_j} = \frac{P_R a_{RB}^2 h_{RB}^2}{\sigma_{B_j}^2}, \tag{12}$$

where γ_{R_j} denotes the sum SNR of the signals from the node $\mathcal{A}$ and node $\mathcal{B}$ to the relay. γ_{AR_j} and γ_{BR_j} indicate the SNR of the links from node $\mathcal{A}$ to the relay and node $\mathcal{B}$ to the relay, respectively. γ_{RA_j} and γ_{RB_j} represent the SNR of the links from the relay to node $\mathcal{A}$ and the relay to node $\mathcal{B}$, respectively.

Similar to the PNC, in the ANC, the relay first decodes the signals received from the source nodes $\mathcal{A}$ and $\mathcal{B}$. However, unlike PNC, the relay applies a power allocation factor θ, where $\theta \in (0, 1)$ [18]. The relay sends its data with power allocation θP_R and $(1 - \theta)P_R$, to the nodes $\mathcal{A}$ and $\mathcal{B}$, respectively. Subsequently, the relay transmits the signal $x_R = \sqrt{P_R} x_C$, where $x_C = \sqrt{1 - \theta} x_A \oplus \sqrt{\theta} x_B$. At the destination nodes, the nodes subtract their previous transmitted data before decoding. For the PLC DF TWR with ANC, the instantaneous SNRs of the signals received at the relay, nodes $\mathcal{A}$, and $\mathcal{B}$ are, respectively, expressed as

$$\gamma_{R_j} = \gamma_{AR_j} + \gamma_{BR_j}, \tag{13}$$

$$\gamma_{AR_j} = \frac{P_A a_{AR}^2 h_{AR}^2}{\sigma_{R_j}^2}, \quad \gamma_{BR_j} = \frac{P_B a_{BR}^2 h_{BR}^2}{\sigma_{R_j}^2}, \tag{14}$$

and

$$\gamma_{RA_j} = \frac{\theta P_R a_{RA}^2 h_{RA}^2}{\sigma_{A_j}^2}, \quad \gamma_{RB_j} = \frac{(1 - \theta) P_R a_{RB}^2 h_{RB}^2}{\sigma_{B_j}^2}. \tag{15}$$

In the next section, we analyze the average sum capacity and the outage probability for the PLC TWR network.

III. PERFORMANCE ANALYSIS

In this section, we analyze the average sum capacity and the outage probability for the AF and DF schemes of the PLC TWR network in subsections III-A and III-B, respectively. We derive the analytic results by utilizing the properties of the log-normal distribution [53], [54]. The channels h_{AR}^2 and h_{BR}^2 are represented by the RVs, X and Y, respectively.

A. AVERAGE SUM CAPACITY

The average sum capacity of an AF TWR configuration is determined as the sum of the individual capacity of each source-relay link. By using (7) and (8), the average sum capacity of the PLC AF TWR is given by

$$C_{AF} = \frac{1}{2}\sum_{j=0}^{1} p_j \mathbb{E}\left[\log_2(1+\gamma_{A_j})\right] + \frac{1}{2}\sum_{j=0}^{1} p_j \mathbb{E}\left[\log_2(1+\gamma_{B_j})\right], \tag{16}$$

where $p_0 = 1-p$, and $p_1 = p$. The pre-log factor $\frac{1}{2}$ exists as the communication is completed in two phases.

Theorem 1: By using the AF TWR, and under the assumption of a log-normal fading channel in the presence of impulsive noise, the average sum capacity of the PLC network is approximated using the Gauss-Laguerre quadrature as

$$C_{AF} \approx \frac{1}{2\ln(2)}\sum_{j=0}^{1}\sum_{m=1}^{M} p_j \frac{\varrho_m}{\iota_m}\left(1-\mathcal{M}_{\mathcal{Y}}(\delta_{m_j})\right)\mathcal{M}_{\mathcal{X}_j}(\delta_{m_j}) + \frac{1}{2\ln(2)}\sum_{j=0}^{1}\sum_{m=1}^{M} p_j \frac{\varrho_m}{\iota_m}\left(1-\mathcal{M}_{\mathcal{K}}(\varepsilon_{m_j})\right)\mathcal{M}_{\mathcal{Z}_j}(\varepsilon_{m_j}), \tag{17}$$

where $\delta_{m_j} = \iota_m/\eta_j$, $\varepsilon_{m_j} = \iota_m/\omega_j$. ϱ_m and ι_m denote the weights and zeros of the M-order Laguerre polynomial, respectively, tabulated in [55, Table 25.9]. The terms η_j, $\mathcal{M}_{\mathcal{X}_j}(\cdot)$, $\mathcal{M}_{\mathcal{Y}}(\cdot)$, ω_j, $\mathcal{M}_{\mathcal{K}}(\cdot)$, and $\mathcal{M}_{\mathcal{Z}_j}(\cdot)$ are defined in (60), (65), (66), (68), (70), and (71), respectively, in Appendix A.

Proof: Please refer to Appendix A ∎

Next, we derive the average sum capacity of the PLC DF TWR with PNC which is defined as [16]

$$C_{DF,PNC} = \mathbb{E}[\min(C_{MAC}, C_A + C_B)], \tag{18}$$

where

$$C_{MAC} = \frac{1}{2}\sum_{j=0}^{1} p_j \log_2(1+\gamma_{R_j}), \tag{19}$$

$$C_A = \frac{1}{2}\sum_{j=0}^{1} p_j \min\left(\log_2(1+\gamma_{BR_j}), \log_2(1+\gamma_{RA_j})\right), \tag{20}$$

and

$$C_B = \frac{1}{2}\sum_{j=0}^{1} p_j \min(\log_2(1+\gamma_{AR_j}), \log_2(1+\gamma_{RB_j})). \tag{21}$$

As can be seen from the equations above, the average capacity is constrained by both the MAC and the BC stages.

Theorem 2: Under the assumption of a log-normal fading channel in the presence of impulsive noise and by using the DF TWR with PNC, the average capacity of the PLC network is given by

$$C_{DF,PNC} = \min\left(\mathbb{E}[C_{MAC}], \mathbb{E}[C_A] + \mathbb{E}[C_B]\right), \tag{22}$$

where $\mathbb{E}[C_{MAC}]$, $\mathbb{E}[C_A]$, and $\mathbb{E}[C_B]$ are approximated in (23), (24), and (25), as shown at the bottom of this page, respectively. The RVs γ_{AR_j} and γ_{BR_j} are respectively distributed as $\gamma_{AR_j} \sim \mathcal{N}(2\mu_X + \xi\ln(P_A a_{AR}^2/\sigma_{R_j}^2), 4\sigma_X^2)$ and $\gamma_{BR_j} \sim \mathcal{N}(2\mu_Y + \xi\ln(P_B a_{BR}^2/\sigma_{R_j}^2), 4\sigma_Y^2)$. The RVs γ_{RA_j} and γ_{RB_j} are

$$\mathbb{E}[C_{MAC}] \approx \frac{1}{2\ln(2)}\sum_{j=0}^{1}\sum_{k=1}^{K} p_j \frac{w_k}{\sqrt{\pi}} \ln\left(1+\exp\left(\frac{\sqrt{8\sigma_{\chi_j}^2}s_k + 2\mu_{\chi_j}}{\xi}\right)\right), \tag{23}$$

$$\mathbb{E}[C_A] \approx \frac{1}{2\ln(2)}\sum_{j=0}^{1} p_j \frac{2}{3}\left[\Phi_{1_j}\left(\mu_{\gamma_{BR_j}}\right) + \Phi_{2_j}\left(\mu_{\gamma_{RA_j}}\right)\right] + \frac{1}{6}\left[\Phi_{1_j}\left(\mu_{\gamma_{BR_j}} + \sqrt{3}\sigma_{\gamma_{BR}}\right) + \Phi_{2_j}\left(\mu_{\gamma_{RA_j}} + \sqrt{3}\sigma_{\gamma_{RA}}\right)\right] + \frac{1}{6}\left[\Phi_{1_j}\left(\mu_{\gamma_{BR_j}} - \sqrt{3}\sigma_{\gamma_{BR}}\right) + \Phi_{2_j}\left(\mu_{\gamma_{RA_j}} - \sqrt{3}\sigma_{\gamma_{RA}}\right)\right], \tag{24}$$

$$\mathbb{E}[C_B] \approx \frac{1}{2\ln(2)}\sum_{j=0}^{1} p_j \frac{2}{3}\left[\Phi_{3_j}\left(\mu_{\gamma_{AR_j}}\right) + \Phi_{4_j}\left(\mu_{\gamma_{RB_j}}\right)\right] + \frac{1}{6}\left[\Phi_{3_j}\left(\mu_{\gamma_{AR_j}} + \sqrt{3}\sigma_{\gamma_{AR}}\right) + \Phi_{4_j}\left(\mu_{\gamma_{RB_j}} + \sqrt{3}\sigma_{\gamma_{RB}}\right)\right] + \frac{1}{6}\left[\Phi_{3_j}\left(\mu_{\gamma_{AR_j}} - \sqrt{3}\sigma_{\gamma_{AR}}\right) + \Phi_{4_j}\left(\mu_{\gamma_{RB_j}} - \sqrt{3}\sigma_{\gamma_{RB}}\right)\right], \tag{25}$$

$$\Phi_{1_j}(x) = \ln\left(1+\exp\left(\frac{x}{\xi}\right)\right) Q\left(\frac{x-\mu_{\gamma_{RA_j}}}{\sigma_{\gamma_{RA}}}\right), \Phi_{2_j}(x) = \ln\left(1+\exp\left(\frac{x}{\xi}\right)\right) Q\left(\frac{x-\mu_{\gamma_{BR_j}}}{\sigma_{\gamma_{BR}}}\right), \tag{26}$$

$$\Phi_{3_j}(x) = \ln\left(1+\exp\left(\frac{x}{\xi}\right)\right) Q\left(\frac{x-\mu_{\gamma_{RB_j}}}{\sigma_{\gamma_{RB}}}\right), \Phi_{4_j}(x) = \ln\left(1+\exp\left(\frac{x}{\xi}\right)\right) Q\left(\frac{x-\mu_{\gamma_{AR_j}}}{\sigma_{\gamma_{AR}}}\right). \tag{27}$$

distributed as $\gamma_{RA_j} \sim \mathcal{N}(2\mu_X + \xi \ln(P_R a_{RA}^2/\sigma_{A_j}^2), 4\sigma_X^2)$, and $\gamma_{RB_j} \sim \mathcal{N}(2\mu_Y + \xi \ln(P_R a_{RB}^2/\sigma_{B_j}^2), 4\sigma_Y^2)$, respectively.

Proof: Please refer to Appendix B ∎

Corollary 1: From *Theorem 2* and by combining (13), (14), and (15), the average sum capacity of the PLC DF TWR with ANC is found as

$$C_{DF,ANC} = \min\left(\mathbb{E}[C_{MAC}], \mathbb{E}[C_A] + \mathbb{E}[C_B]\right), \quad (28)$$

where $\mathbb{E}[C_{MAC}]$, $\mathbb{E}[C_A]$, and $\mathbb{E}[C_B]$ are approximated in (23), (24), and (25), respectively. For calculating the average sum capacity of the PLC DF TWR with ANC, the RVs γ_{AR_j} and γ_{BR_j} are distributed as $\gamma_{AR_j} \sim \mathcal{N}(2\mu_X + \xi \ln(P_A a_{AR}^2/\sigma_{R_j}^2), 4\sigma_X^2)$ and $\gamma_{BR_j} \sim \mathcal{N}(2\mu_Y + \xi \ln(P_B a_{BR}^2/\sigma_{R_j}^2), 4\sigma_Y^2)$, respectively. Also, the RVs γ_{RA_j} and γ_{RB_j} are distributed as $\gamma_{RA_j} \sim \mathcal{N}(2\mu_X + \xi \ln(\theta P_R a_{RA}^2/\sigma_{A_j}^2), 4\sigma_X^2)$, and $\gamma_{RB_j} \sim \mathcal{N}(2\mu_Y + \xi \ln((1-\theta) P_R a_{RB}^2/\sigma_{B_j}^2), 4\sigma_Y^2)$, respectively.

B. OUTAGE PROBABILITY

For the TWR, both data symbols must be successfully decoded at both the destination nodes otherwise an outage occurs. Let $\gamma_{th} = 2^{2R_{th}} - 1$, where γ_{th} and R_{th} are the target SNR and rate thresholds, respectively. To correctly decode the received signal in the MAC phase for the DF protocol, the relay applies successive interference cancellation (SIC) [46]. The decoding process occurs iteratively, where one data symbol is considered as an interference to the other. For instance, to decode the signal from node $\mathcal{A}$, the signal from node $\mathcal{B}$ is considered as noise. After successfully decoding x_A, it is subtracted from the received signal and x_B can now be decoded.

The outage probability of the PLC AF TWR in the presence of impulsive noise is defined as

$$P_{out}^{AF} = p_0 \cdot \Pr\left(\min(\gamma_{A_0}, \gamma_{B_0}) < \gamma_{th}\right) + p_1 \cdot \Pr\left(\min(\gamma_{A_1}, \gamma_{B_1}) < \gamma_{th}\right). \quad (29)$$

Theorem 3: Considering the PLC with log-normal fading channels in the presence of impulsive noise, the outage probability of the AF TWR is determined as

$$P_{out}^{AF} = \sum_{j=0}^{1} p_j (I_{A_j} + I_{B_j} - I_{AB_j}), \quad (30)$$

where I_{A_j}, I_{B_j}, and I_{AB_j} are expressed in (31) - (38) shown at the bottom of the next page where $\epsilon_1 = P_B a_{BR}^2$, $\epsilon_2 = \beta^2 a_{RA}^2$, $\vartheta_1 = P_A a_{AR}^2$, and $\vartheta_2 = \beta^2 a_{RB}^2$. Λ_{X_j}, and Λ_{Y_j}, are defined in (101), and (102), respectively, in Appendix C. For (31), as shown at the bottom of the next page, the RVs $\mathcal{Y}$ and $\mathcal{X}_j$ are distributed as $\mathcal{Y} \sim \mathcal{N}(2\mu_Y + \xi \ln(\epsilon_1\epsilon_2), 4\sigma_Y^2)$, and $\mathcal{X}_j \sim \mathcal{N}(-2\mu_X + \xi \ln(\sigma_{A_j}^2), 4\sigma_X^2)$, respectively. For (32), as shown at the bottom of the next page, the RVs $\mathcal{K}$ and $\mathcal{Z}_j$ are distributed as $\mathcal{K} \sim \mathcal{N}(2\mu_X + \xi \ln(\vartheta_1\vartheta_2), 4\sigma_X^2)$, and $\mathcal{Z}_j \sim \mathcal{N}(-2\mu_Y + \xi \ln(\sigma_{B_j}^2), 4\sigma_Y^2)$, respectively.

Proof: The proof is given in Appendix C ∎

Next, we derive the outage probability of the PLC DF TWR system. With SIC decoding, the instantaneous SNRs of the PLC DF TWR with PNC are determined as [18]

$$\gamma_{AR_j}^{DF} = \frac{P_A a_{AR}^2 h_{AR}^2}{P_B a_{BR}^2 h_{BR}^2 + \sigma_{R_j}^2}, \quad \gamma_{AR_j}^{SIC} = \frac{P_A a_{AR}^2 h_{AR}^2}{\sigma_{R_j}^2},$$
$$\gamma_{BR_j}^{DF} = \frac{P_B a_{BR}^2 h_{BR}^2}{P_A a_{AR}^2 h_{AR}^2 + \sigma_{R_j}^2}, \quad \gamma_{BR_j}^{SIC} = \frac{P_B a_{BR}^2 h_{BR}^2}{\sigma_{R_j}^2},$$
$$\gamma_{RA_j}^{DF} = \frac{P_R a_{RA}^2 h_{RA}^2}{\sigma_{A_j}^2}, \quad \gamma_{RB_j}^{DF} = \frac{P_R a_{RB}^2 h_{RB}^2}{\sigma_{B_j}^2}. \quad (39)$$

The outage probability of the DF TWR with PNC is obtained as [46]

$$P_{out}^{DF,PNC} = \sum_{j=0}^{1} p_j P_{out_j}^{DF,PNC} \quad (40)$$

where

$$P_{out_j}^{DF,PNC} = 1 - \Pr(\{\{\gamma_{AR_j}^{DF} \geq \gamma_{th}\} \cap \{\gamma_{BR_j}^{SIC} \geq \gamma_{th}\} \cap \{\gamma_{RA_j}^{DF} \geq \gamma_{th}\} \cap \{\gamma_{RB_j}^{DF} \geq \gamma_{th}\}\} \cup \{\{\gamma_{BR_j}^{DF} \geq \gamma_{th}\} \cap \{\gamma_{AR_j}^{SIC} \geq \gamma_{th}\} \cap \{\gamma_{RA_j}^{DF} \geq \gamma_{th}\} \cap \{\gamma_{RB_j}^{DF} \geq \gamma_{th}\}\}). \quad (41)$$

Theorem 4: For PLC log-normal channels in the presence of impulsive noise, the outage probability of the DF TWR with PNC is written as

$$P_{out}^{DF,PNC} = 1 - \sum_{j=0}^{1} p_j \left(\sum_{\zeta=1}^{2} \int_{\Delta_{\zeta_j}}^{\infty} f_\zeta \Omega_{\zeta_j} \right). \quad (42)$$

The terms Δ_{1_j}, Δ_{2_j}, f_1, f_2, Ω_{1_j}, and Ω_{2_j} are expressed, respectively, as

$$\Delta_{1_j} = \frac{\sigma_{B_j}^2 \gamma_{th}}{P_R a_{RB}^2}, \quad (43)$$

$$\Delta_{2_j} = \frac{\sigma_{A_j}^2 \gamma_{th}}{P_R a_{RA}^2}, \quad (44)$$

$$f_1 = \frac{\xi}{y\sqrt{8\pi\sigma_X^2}} \exp\left(-\frac{(\xi \ln(y) - 2\mu_X)^2}{8\sigma_X^2}\right), \quad (45)$$

$$f_2 = \frac{\xi}{x\sqrt{8\pi\sigma_Y^2}} \exp\left(-\frac{(\xi \ln(x) - 2\mu_Y)^2}{8\sigma_Y^2}\right), \quad (46)$$

$$\Omega_{1_j} = Q\left(\frac{\xi \ln\left(\frac{\gamma_{th} P_B a_{BR}^2 y + \gamma_{th}\sigma_{R_j}^2}{P_A a_{AR}^2}\right) - 2\mu_Y}{2\sigma_Y}\right) dy, \quad (47)$$

and

$$\Omega_{2_j} = Q\left(\frac{\xi \ln\left(\frac{\gamma_{th} P_A a_{AR}^2 x + \gamma_{th}\sigma_{R_j}^2}{P_B a_{BR}^2}\right) - 2\mu_X}{2\sigma_X}\right) dx. \quad (48)$$

Proof: The proof is given in Appendix D ∎

Corollary 2: By utilizing *Theorem 4*, the outage probability of the PLC DF TWR with ANC in the presence of impulsive noise is obtained as

$$P_{out}^{DF,ANC} = 1 - \sum_{j=0}^{1} p_j \left(\sum_{\zeta=1}^{2} \int_{\Delta_{\zeta_j}}^{\infty} f_\zeta \Omega_{\zeta_j} \right). \tag{49}$$

For the PLC TWR with ANC, the terms f_1, f_2, Ω_{1_j}, and Ω_{2_j} are the same as the PNC case. However, Δ_{1_j} and Δ_{2_j} are defined as

$$\Delta_{1_j} = \frac{\sigma_{B_j}^2 \gamma_{th}}{(1-\theta) P_R a_{RB}^2}, \tag{50}$$

and

$$\Delta_{2_j} = \frac{\sigma_{A_j}^2 \gamma_{th}}{\theta P_R a_{RA}^2}. \tag{51}$$

It is worth mentioning that the derived outage probability expressions for the AF and DF TWR contain integrals that are difficult to be expressed in closed-form because of the intractable form of the Q function expressions in (35), (37), (47), and (48).[3]

IV. HYBRID PLC/WIRELESS PERFORMANCE ANALYSIS

To improve the reliability of the PLC network, we investigate the performance of an HPW network in the TWR where the source nodes transmit their signals through two independent communication links, i.e., PLC and wireless communications. For the wireless link, we assume the Rayleigh fading,

[3] In [33], [56], integrals involving the product of an exponential and Q function are solved by the use of an appropriate change of variable and approximating either the exponential function or the Q function. However, in (35), (37), (47), and (48), the Q function in the integrals is difficult to approximate due to the complicated form of the embedded (ln) expression.

$$I_{A_j} = 1 - \frac{2}{3} Q\left(\frac{\Phi_{5_j}(\mu_{\mathcal{X}_j}) - \mu_{\mathcal{Y}}}{\sigma_{\mathcal{Y}}} \right) - \frac{1}{6} Q\left(\frac{\Phi_{5_j}(\mu_{\mathcal{X}_j} + \sqrt{3}\sigma_{\mathcal{X}}) - \mu_{\mathcal{Y}}}{\sigma_{\mathcal{Y}}} \right) - \frac{1}{6} Q\left(\frac{\Phi_{5_j}(\mu_{\mathcal{X}_j} - \sqrt{3}\sigma_{\mathcal{X}}) - \mu_{\mathcal{Y}}}{\sigma_{\mathcal{Y}}} \right), \tag{31}$$

$$I_{B_j} = 1 - \frac{2}{3} Q\left(\frac{\Phi_{6_j}(\mu_{\mathcal{Z}_j}) - \mu_{\mathcal{K}}}{\sigma_{\mathcal{K}}} \right) - \frac{1}{6} Q\left(\frac{\Phi_{6_j}(\mu_{\mathcal{Z}_j} + \sqrt{3}\sigma_{\mathcal{Z}}) - \mu_{\mathcal{K}}}{\sigma_{\mathcal{K}}} \right) - \frac{1}{6} Q\left(\frac{\Phi_{6_j}(\mu_{\mathcal{Z}_j} - \sqrt{3}\sigma_{\mathcal{Z}}) - \mu_{\mathcal{K}}}{\sigma_{\mathcal{K}}} \right), \tag{32}$$

$$\Phi_{5_j}(x) = \xi \ln\left(\gamma_{th} \exp\left(\frac{x}{\xi} \right) + \gamma_{th}\eta_j \right), \Phi_{6_j}(x) = \xi \ln\left(\gamma_{th} \exp\left(\frac{x}{\xi} \right) + \gamma_{th}\omega_j \right), \tag{33}$$

$$I_{AB_j} = I_{1_j} + I_{2_j}, \tag{34}$$

$$\begin{aligned} I_{1_j} = {} & \frac{2}{3} Q\left(\frac{\Phi_{7_j}(2\mu_X) - 2\mu_Y}{2\sigma_Y} \right) + \frac{1}{6} Q\left(\frac{\Phi_{7_j}(2\mu_X + 2\sqrt{3}\sigma_X) - 2\mu_Y}{2\sigma_Y} \right) + \frac{1}{6} Q\left(\frac{\Phi_{7_j}(2\mu_X - 2\sqrt{3}\sigma_X) - 2\mu_Y}{2\sigma_Y} \right) \\ & - \frac{2}{3} Q\left(\frac{\Phi_{8_j}(2\mu_X) - 2\mu_Y}{2\sigma_Y} \right) - \frac{1}{6} Q\left(\frac{\Phi_{8_j}(2\mu_X + 2\sqrt{3}\sigma_X) - 2\mu_Y}{2\sigma_Y} \right) - \frac{1}{6} Q\left(\frac{\Phi_{8_j}(2\mu_X - 2\sqrt{3}\sigma_X) - 2\mu_Y}{2\sigma_Y} \right) \\ & - \frac{1}{2} \left[Q\left(\frac{\Phi_{9_j}(\Lambda_{X_j}) - 2\mu_Y}{2\sigma_Y} \right) \right]^2 + \int_{\Lambda_{X_j}}^{\infty} \frac{\xi}{x\sqrt{8\pi\sigma_X^2}} \exp\left(-\frac{(\xi \ln(x) - 2\mu_X)^2}{8\sigma_X^2} \right) Q\left(\frac{\xi \ln\left(\frac{\gamma_{th}}{\epsilon_1} \left(\sigma_{R_j}^2 + \frac{\sigma_{A_j}^2}{\epsilon_2 x} \right) \right) - 2\mu_Y}{2\sigma_Y} \right) dx. \end{aligned} \tag{35}$$

$$\Phi_{7_j}(x) = \xi \ln\left(\frac{\Lambda_{Y_j}}{\Lambda_{X_j}} \exp(x/\xi) \right), \Phi_{8_j}(x) = \xi \ln\left(\frac{\gamma_{th}}{\epsilon_1} \left(\sigma_{R_j}^2 + \frac{\sigma_{A_j}^2}{\epsilon_2 \exp(x/\xi)} \right) \right), \Phi_{9_j}(x) = \xi \ln\left(\frac{\Lambda_{Y_j}}{\Lambda_{X_j}} x \right), \tag{36}$$

$$\begin{aligned} I_{2_j} = {} & \frac{2}{3} Q\left(\frac{\Phi_{11_j}(2\mu_Y) - 2\mu_X}{2\sigma_X} \right) + \frac{1}{6} Q\left(\frac{\Phi_{11_j}(2\mu_Y + 2\sqrt{3}\sigma_Y) - 2\mu_X}{2\sigma_X} \right) + \frac{1}{6} Q\left(\frac{\Phi_{11_j}(2\mu_Y - 2\sqrt{3}\sigma_Y) - 2\mu_X}{2\sigma_X} \right) \\ & - \frac{2}{3} Q\left(\frac{\Phi_{12_j}(2\mu_Y) - 2\mu_X}{2\sigma_X} \right) - \frac{1}{6} Q\left(\frac{\Phi_{12_j}(2\mu_Y + 2\sqrt{3}\sigma_Y) - 2\mu_X}{2\sigma_X} \right) - \frac{1}{6} Q\left(\frac{\Phi_{12_j}(2\mu_Y - 2\sqrt{3}\sigma_Y) - 2\mu_X}{2\sigma_X} \right) \\ & - \frac{1}{2} \left[Q\left(\frac{\Phi_{13_j}(\Lambda_{Y_j}) - 2\mu_X}{2\sigma_X} \right) \right]^2 + \int_{\Lambda_{Y_j}}^{\infty} \frac{\xi}{y\sqrt{8\pi\sigma_Y^2}} \exp\left(-\frac{(\xi \ln(y) - 2\mu_Y)^2}{8\sigma_Y^2} \right) Q\left(\frac{\xi \ln\left(\frac{\gamma_{th}}{\vartheta_1} \left(\sigma_{R_j}^2 + \frac{\sigma_{B_j}^2}{\vartheta_2 y} \right) \right) - 2\mu_X}{2\sigma_X} \right) dy. \end{aligned} \tag{37}$$

$$\Phi_{11_j}(x) = \xi \ln\left(\frac{\Lambda_{X_j}}{\Lambda_{Y_j}} \exp(x/\xi) \right), \Phi_{12_j}(x) = \xi \ln\left(\frac{\gamma_{th}}{\vartheta_1} \left(\sigma_{R_j}^2 + \frac{\sigma_{B_j}^2}{\vartheta_2 \exp(x/\xi)} \right) \right), \Phi_{13_j}(x) = \xi \ln\left(\frac{\Lambda_{X_j}}{\Lambda_{Y_j}} x \right). \tag{38}$$

where the channel gain $|h_i|^2$ has the PDF given as [49]

$$f_{|h_i|^2}(z) = \frac{1}{\lambda_i} \exp\left(-\frac{z}{\lambda_i}\right), \quad z \geq 0, \tag{52}$$

where the mean λ_i is modeled as $\lambda_i = \sqrt{d_i^{-\alpha}}$ and α is the pathloss exponent. Consequently, the outage probability of the HPW AF TWR and the HPW DF TWR are expressed, respectively, as

$$P^{AF}_{out,HPW} = P^{AF}_{out,P} \cdot P^{AF}_{out,W}, \tag{53}$$

and

$$P^{DF}_{out,HPW} = P^{DF}_{out,P} \cdot P^{DF}_{out,W}, \tag{54}$$

where $P^{AF}_{out,P}$, $P^{AF}_{out,W}$, $P^{DF}_{out,P}$, and $P^{DF}_{out,W}$ indicate the outage probability of the AF PLC link, AF wireless link, DF PLC link, and DF wireless links, respectively.

For the AF TWR, the gain of the wireless link is given as

$$\kappa = \sqrt{\frac{P_R}{(P_A \mathbb{E}[h^2_{AR}] + P_B \mathbb{E}[h^2_{BR}] + \sigma^2_{R_0})}}. \tag{55}$$

In the BC phase, the resultant SNRs at the nodes $\mathcal{A}$ and $\mathcal{B}$ are, respectively, given by

$$\gamma_A = \frac{P_B h^2_{RA} h^2_{BR}}{h^2_{RA}\sigma^2_{R_0} + \psi_1}, \tag{56}$$

and

$$\gamma_B = \frac{P_A h^2_{AR} h^2_{RB}}{h^2_{RB}\sigma^2_{R_0} + \psi_2}, \tag{57}$$

where $\psi_1 = \sigma^2_{A_0}/\kappa^2$ and $\psi_2 = \sigma^2_{B_0}/\kappa^2$.

The outage probability of the AF TWR in the wireless link is given by [57]

$$\begin{aligned} P^{AF}_{out,W} &= 1 + \exp\left(-\frac{X_0}{\lambda_X} - \frac{Y_0}{\lambda_Y}\right) \\ &\quad - \exp\left(-\frac{\gamma_{th}\psi_2}{P_A\lambda_X}\right)\sqrt{\frac{4\gamma_{th}\sigma^2_{R_0}}{P_A\lambda_X\lambda_Y}} K_1\left(\sqrt{\frac{4\gamma_{th}\sigma^2_{R_0}}{P_A\lambda_X\lambda_Y}}\right) \\ &\quad - \exp\left(-\frac{\gamma_{th}\psi_1}{P_B\lambda_Y}\right)\sqrt{\frac{4\gamma_{th}\sigma^2_{R_0}}{P_B\lambda_X\lambda_Y}} K_1\left(\sqrt{\frac{4\gamma_{th}\sigma^2_{R_0}}{P_B\lambda_X\lambda_Y}}\right) \\ &\quad + \sum_{c=0}^{2} \frac{\mathcal{H}^{(c)}_{X,Y}(v_X)}{c!(c+1)}\left((V_X - v_X)^{c+1} - (-v_X)^{c+1}\right) \\ &\quad + \sum_{c=0}^{2} \frac{\mathcal{H}^{(c)}_{Y,X}(v_Y)}{c!(c+1)}\left(V_Y - v_Y)^{c+1} - (-v_Y)^{c+1}\right), \end{aligned} \tag{58}$$

where X_0, Y_0, $\mathcal{H}_{X,Y}(\cdot)$, V_X, v_X, $\mathcal{H}_{Y,X}(\cdot)$, V_Y, and v_Y are defined in [57, eq. (11)] and $K_1(\cdot)$ is the modified Bessel function of the second kind.

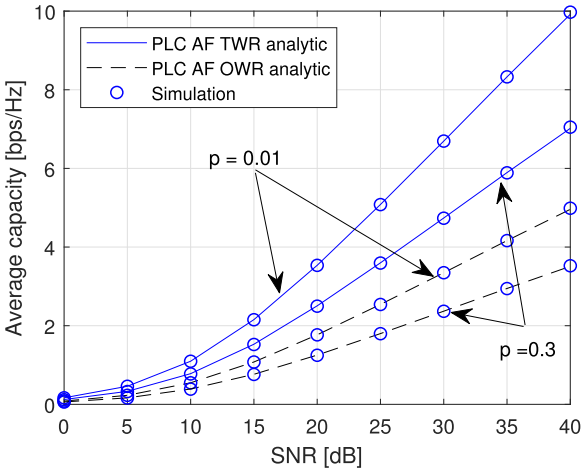

FIGURE 2. Average capacity versus input SNR for PLC AF relays ($\mu_{AR} = \mu_{BR} = 0$dB and $\sigma_{AR} = \sigma_{BR} = 1$dB).

For the DF TWR, we consider only the PNC case, for brevity. For the wireless link, the outage probability of DF TWR in a Rayleigh fading is expressed as [18]

$$\begin{aligned} P^{DF}_{out,W} &= 1 - \frac{P_A\lambda_X}{P_A\lambda_X + P_B\lambda_Y\gamma_{th}} \\ &\quad \times \exp\left(-\frac{\gamma_{th}\left(P_A\lambda_X\sigma^2_{B_0} + P_R\lambda_Y\sigma^2_{R_0} + P_B\lambda_Y\sigma^2_{B_0}\gamma_{th}\right)}{P_A P_R \lambda_X\lambda_Y}\right) \\ &\quad - \frac{P_B\lambda_Y}{P_B\lambda_Y + P_A\lambda_X\gamma_{th}} \\ &\quad \times \exp\left(-\frac{\gamma_{th}\left(P_B\lambda_Y\sigma^2_{A_0} + P_R\lambda_X\sigma^2_{R_0} + P_A\lambda_X\sigma^2_{A_0}\gamma_{th}\right)}{P_B P_R \lambda_X\lambda_Y}\right). \end{aligned} \tag{59}$$

In the next section, we provide numerical results to corroborate our analysis.

V. SIMULATION RESULTS

This section presents the numerical results to validate our analysis through Monte Carlo simulations averaged over 10^6 channel realizations. Here, we set the power of the nodes as $P_A = P_B = P_R = 1$W and the node noise variances as $\sigma^2_{A_j} = \sigma^2_{B_j} = \sigma^2_{R_j}$. The SINR is set as -10dB where SNR $= 10\log_{10}(1/\sigma^2_G)$ and SINR $= 10\log_{10}(1/\sigma^2_I)$ [30]. The power line attenuation model has the following parameters: $b_0 = 9.4\times10^{-3}$, $b_1 = 4.2\times10^{-7}$, $k = 0.7$, and $f = 30$MHz [30]. Unless otherwise stated, the distance between node $\mathcal{A}$ and the relay $\mathcal{R}$, and the relay $\mathcal{R}$ and node $\mathcal{B}$ are set to be equidistant, that is, $d_{AR} = d_{BR} = 50$m. For the AF TWR, the relay gains, β and κ, are chosen to be 1.

Fig. 2 shows the average capacity of the AF scheme versus the input SNR for different values of impulsive noise probability p. For all channels, we use $\mu_{AR} = \mu_{BR} = 0$dB, $\sigma_{AR} = \sigma_{BR} = 1$dB. It can be observed that our analytic

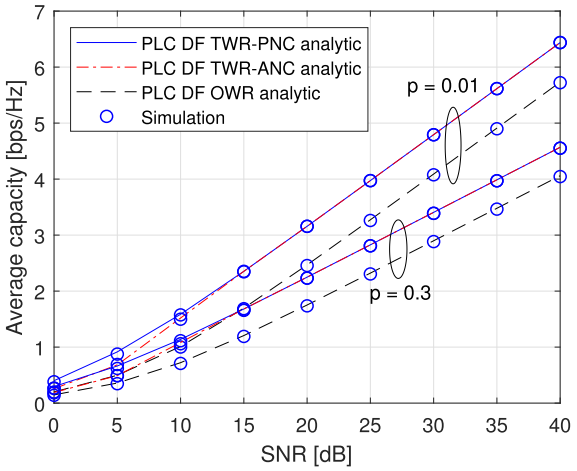

FIGURE 3. Average capacity versus input SNR for PLC DF relays ($\mu_{AR} = \mu_{BR} = 0$dB and $\sigma_{AR} = \sigma_{BR} = 1$dB).

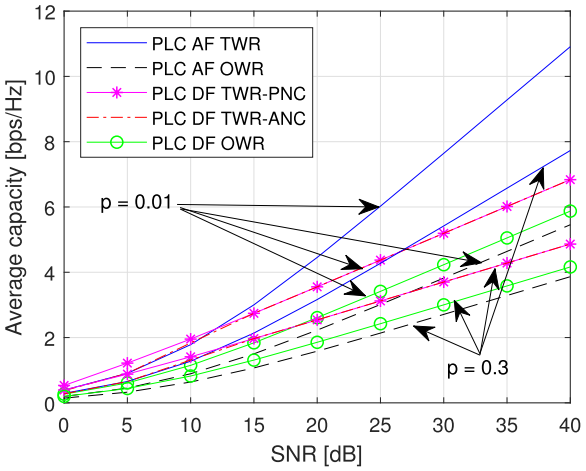

FIGURE 4. Average capacity versus input SNR for various PLC relays ($\mu_{AR} = \mu_{BR} = 3$dB and $\sigma_{AR} = \sigma_{BR} = 2$dB).

results obtained by (17) are highly accurate compared to the Monte Carlo simulations. Also, p has a debilitating effect on the average capacity of the system. Higher p leads to lower average capacity since more of the received data is corrupted by the impulsive noise. Comparing the OWR and the TWR, significant gains can be obtained by the bidirectional communication used in our system. For example, at SNR $=$ 30 dB and $p = 0.01$, the TWR achieves a rate gain of about 3.5bps/Hz over its OWR counterpart.

Next, Fig. 3 compares the average capacity for the PLC DF TWR and OWR. In particular, we compare PNC and ANC for the DF protocol using (22) and (28), respectively. Due to the symmetric nature of the proposed PLC TWR, we set the ANC power allocation factor as $\theta = 0.5$. We use the following parameters: $\mu_{AR} = \mu_{BR} = 0$dB, $\sigma_{AR} = \sigma_{BR} = 1$dB. We observe that, in the low SNR region, i.e., 0-15dB, the PNC scheme outperforms ANC since the data symbols are transmitted with full power at the relay. However, the performance gap reduces as the SNR increases and the two schemes subsequently achieve the same performance. This is because, at low SNR, the average capacity is limited by the BC phase where the power allocation occurs. However, as the SNR increases, the average capacity is limited by the MAC phase. Since the power allocation is not implemented in the MAC phase, the average capacity achieved by the PNC and ANC schemes becomes equal. As expected, the PLC DF TWR outperforms the PLC DF OWR in terms of the average capacity.

Fig. 4 depicts the average capacity comparison between the OWR and the TWR for the various protocols. For all channels, we have $\mu_{AR} = \mu_{BR} = 3$dB and $\sigma_{AR} = \sigma_{BR} = 2$dB and $d_{AR} = d_{BR} = 100$m. It can be observed from the figure that, in the low SNR region, the PLC DF TWR outperforms the PLC AF TWR. This is, however, not the case in the high SNR regime where the AF TWR achieves a higher average capacity than the DF TWR. This is because the joint decoding of both data symbols transmitted in the MAC phase for the DF TWR limits the achievable capacity in the high SNR regime. Due to the fact that the average capacity of the DF protocol is always limited by one of the two phases, the DF TWR only shows a marginal gain over its OWR counterpart. However, the average capacity of the AF TWR is two times the average capacity of the AF OWR since it is not subjected to this limitation. Also, there exists a cross-over point where the AF protocol begins to outperforms the DF protocol, i.e. 12dB for $p = 0.01$. It is therefore vital to design relays that employ a hybrid AF/DF protocol in PLC networks.

The outage probability of the AF protocol versus the input SNR for different values of p is demonstrated in Fig. 5. Here, the rate threshold for the OWR and TWR is set as $R_{th} =$ 1bps/Hz and $\mu_{AR} = \mu_{BR} = 3$dB and $\sigma_{AR} = \sigma_{BR} = 5$dB. It is shown that the analytic results obtained by using (30) are tight compared with the Monte Carlo simulations. We can observe that the outage probability performance of the PLC AF TWR is inferior to its OWR counterpart. This is because, in the TWR, either $\gamma_A < \gamma_{th}$ or $\gamma_B < \gamma_{th}$ will cause an outage. However, the performance gap reduces as the SNR increases.

Fig. 6 illustrates the outage probability performance of the PLC DF OWR and TWR with PNC and ANC as a function of the input SNR. Also, we set the outage rate threshold as $R_{th} = 1$bps/Hz. Here, we set the mean and variance as $\mu_{AR} = \mu_{BR} = 3$dB and $\sigma_{AR} = \sigma_{BR} = 5$dB, respectively. Using (42) and (49), the results show that the outage probability of the TWR is degraded and severely interference limited. This is due to the SIC decoding strategy in the MAC phase where one data symbol is considered as interference to decode the other data symbol as shown in (39). The outage probability for both ANC and PNC, therefore, hits a high error floor as the SNR increases. Consequently, for all values of p, the outage probability performance of the OWR is superior to the TWR. Compared to ANC, PNC can improve the outage performance of the PLC DF TWR. This is because the relay transmits at maximum power with PNC. It is also worth

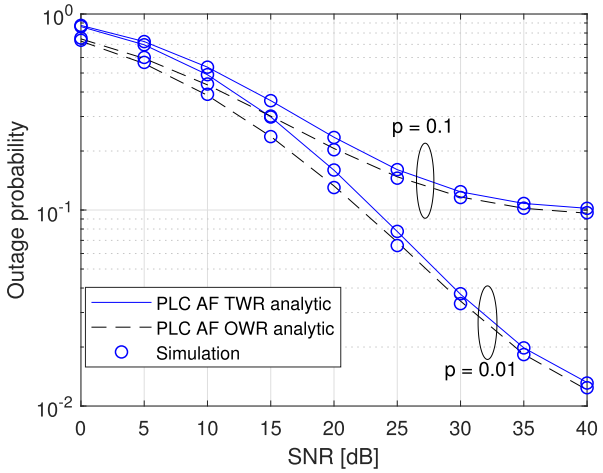

FIGURE 5. Outage probability versus input SNR for PLC AF relays ($\mu_{AR} = \mu_{BR} = 3$dB, $\sigma_{AR} = \sigma_{BR} = 5$dB and $R_{th} = 1$bps/Hz).

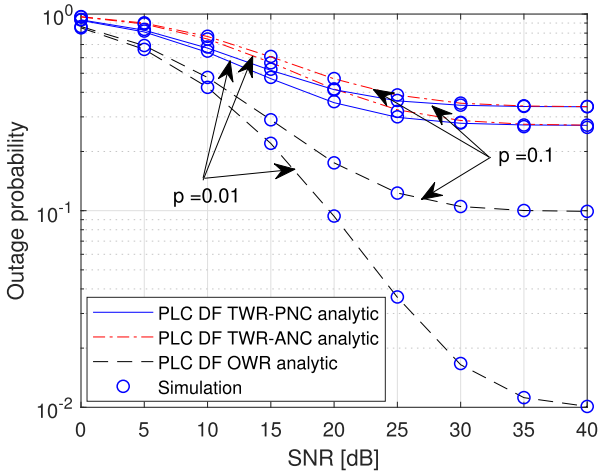

FIGURE 6. Outage probability versus input SNR for PLC DF relays ($\mu_{AR} = \mu_{BR} = 3$dB, $\sigma_{AR} = \sigma_{BR} = 5$dB and $R_{th} = 1$bps/Hz).

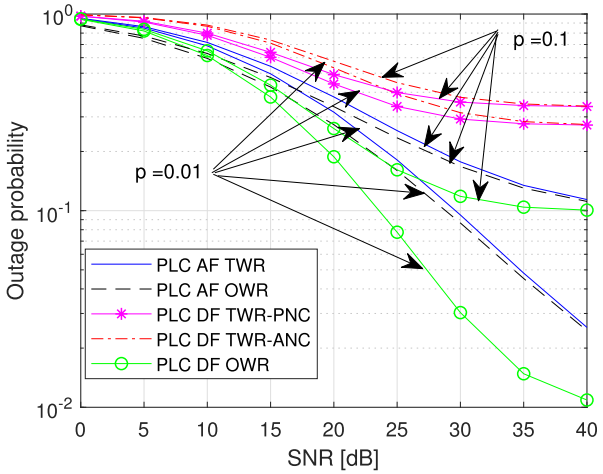

FIGURE 7. Outage probability versus input SNR for various relays ($\mu_{AR} = \mu_{BR} = 1$dB, $\sigma_{AR} = \sigma_{BR} = 5$dB and $R_{th} = 1$bps/Hz).

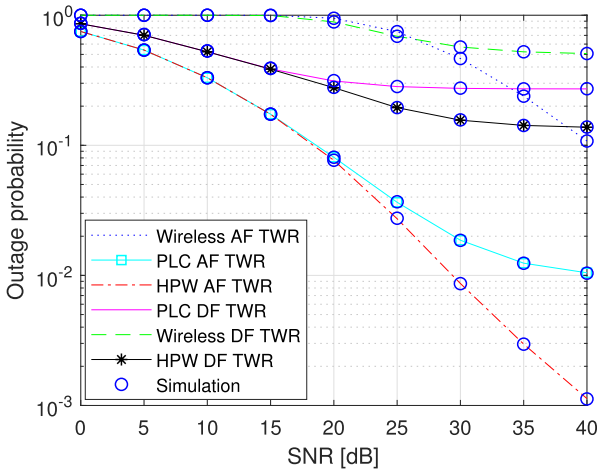

FIGURE 8. Outage probability versus input SNR ($\mu_{AR} = \mu_{BR} = 3$dB, $\sigma_{AR} = \sigma_{BR} = 5$dB and $R_{th} = 1$bps/Hz).

noting that a higher p will result in higher outage probability for both the OWR and the TWR.

Fig. 7 compares the outage probabilities of AF and DF in PLC TWRs. We use the following parameters: $\mu_{AR} = \mu_{BR} = 1$dB, $\sigma_{AR} = \sigma_{BR} = 5$dB and $R_{th} = 1$ bps/Hz. From the figure, the PLC DF OWR has the best outage probability while the PLC DF TWR with ANC has the worst outage probability. Again, the power allocation impacts the overall outage probability of the PLC DF TWR with ANC. Therefore, to achieve lower outage probability in the PLC DF TWR, PNC is preferred to ANC. In addition, the outage probability performance of the AF TWR is generally superior to the DF TWR especially at high SNR where the outage probability of the DF TWR hits an error floor.

In the following, we investigate the outage probability performance of the HPW TWR. For Fig. 8, we use the following parameters: $p = 0.01$, $d_{AR} = d_{BR} = 10$m, $\mu_{AR} = \mu_{BR} = 3$dB, $\sigma_{AR} = \sigma_{BR} = 5$dB, $\alpha = 2$, and $R_{th} = 1$bps/Hz. Fig. 8 shows the outage probability comparison of the TWR for PLC/wireless diversity. The outage probability of the HPW AF TWR is plotted using (53). As can be observed, the AF PLC TWR has a lower outage probability than its wireless counterpart. This is consistent with the results reported in [10]. Furthermore, the outage performance is enhanced in the AF TWR by the introduction of the additional wireless link. For example at an outage probability of 10^{-2}, the HPW AF TWR shows a 10dB gain over the PLC only system. The quality of the HPW TWR is determined by the link with a lower outage probability, .i.e. the PLC link. We can observe from the figure that it is convenient to use the HPW TWR when the input SNR $\geq$ 20dB since it possesses the best outage probability performance. The outage probability of the HPW DF TWR is plotted using (54). Here, the outage probability performance achieved by the HPW DF TWR is superior to both the PLC only and wireless only transmission links. Diversity is achieved by employing the HPW system. From the results, HPW diversity proves useful in designing and meeting new QoS requirements in applications where PLC only systems cannot meet set targets. HPW diversity

is also a potential solution in the interconnected Internet of Things (IoT) applications to increase reliability.

VI. CONCLUSION

In this paper, we have analyzed the performance of a PLC TWR over log-normal channels. Analytic expressions for the average capacity and the outage probability for both the AF and the DF protocols have been derived. Our analytic results have been shown to be very tight when compared with Monte Carlo simulations. The comparison of OWR and TWR showed that the average capacity is improved in TWR. Thus, the spectral efficiency loss incurred by OWR is effectively compensated by using the TWR. However, the outage probability of the TWR is inferior to that of the OWR. In the DF protocol, DF TWR with PNC is the preferred networking scheme in terms of average capacity in the low SNR regime and the outage probability. DF TWR with ANC achieves the same average capacity as PNC in the high SNR region. From the analysis, it is shown that the impulsive noise severely limits the performance of the PLC network. To further improve the outage performance of the TWR, we have analyzed the outage performance of a hybrid PLC/wireless system where all the nodes are equipped with PLC and wireless capabilities. The results have shown that the outage probability of the HPW TWR shows significant improvements compared to both the PLC only and the wireless only systems.

Imperfect SIC due to imperfect channel estimation and energy efficiency analysis can be interesting topics for future research.

APPENDIX A
PROOF OF THEOREM 1

To find the average capacity $\mathbb{E}[C_A]$, we can write (7) in a form amenable to analysis. We have

$$\gamma_{Aj} = \frac{\mathcal{Y}}{\mathcal{X}_j + \eta_j}, \tag{60}$$

where $\mathcal{Y} = \epsilon_1\epsilon_2 Y$, $\epsilon_1 = P_B a_{BR}^2$, $\epsilon_2 = \beta^2 a_{RA}^2$, $\mathcal{X}_j = \sigma_{Aj}^2 X^{-1}$, and $\eta_j = \epsilon_2\sigma_{Rj}^2$. Hence, the average capacity at node $\mathcal{A}$ can be reexpressed as

$$\mathbb{E}[C_A] = \frac{1}{2}\sum_{j=0}^{1} p_j \mathbb{E}\left[\log_2\left(1 + \frac{\mathcal{Y}}{\mathcal{X}_j + \eta_j}\right)\right]. \tag{61}$$

To evaluate the average capacity in (61), we use the following. It is shown in [58] that for any RV $u, v > 0$,

$$\mathbb{E}\left[\ln(1 + \frac{u}{v})\right] = \int_0^\infty \frac{1}{z}(1 - \mathcal{M}_u(z))\mathcal{M}_v(z)dz. \tag{62}$$

Using the defintion in (62), the average capacity at node $\mathcal{A}$, $\mathbb{E}[C_A]$, is obtained as

$$\mathbb{E}[C_A] = \frac{1}{2\ln(2)}\sum_{j=0}^{1} p_j \int_0^\infty \frac{1}{z}(1 - \mathcal{M}_{\mathcal{Y}}(z))e^{(-\eta_j z)}\mathcal{M}_{\mathcal{X}_j}(z)dz. \tag{63}$$

According to [53], the Gauss-Hermite representation of the MGF of any log-normally distributed channel h is given as

$$\mathcal{M}_h(z) \simeq \sum_{k=1}^{K} \frac{w_k}{\sqrt{\pi}} \exp\left[-z\exp\left(\frac{\sqrt{2}\sigma_h s_k + \mu_h}{\xi}\right)\right], \tag{64}$$

where w_k and s_k denote the weights and zeros of the K-order Hermite polynomial, respectively tabulated in [55, Table 25.10]. A higher value of K corresponds to greater computational accuracy. Using the properties of the log-normal distribution where $X^{-1} \sim \mathcal{N}(-2\mu_X, 4\sigma_X^2)$ and $Y \sim \mathcal{N}(2\mu_Y, 4\sigma_Y^2)$, the MGFs of $\mathcal{X}_j$ and $\mathcal{Y}$ are determined, respectively, as

$$\mathcal{M}_{\mathcal{X}_j}(z) \simeq \sum_{k=1}^{K} \frac{w_k}{\sqrt{\pi}} \times \exp\left[-\sigma_{Aj}^2 z\exp\left(-\frac{2\sqrt{2}\sigma_X s_k + 2\mu_X}{\xi}\right)\right], \tag{65}$$

and

$$\mathcal{M}_{\mathcal{Y}}(z) \simeq \sum_{k=1}^{K} \frac{w_k}{\sqrt{\pi}} \times \exp\left[-\epsilon_1\epsilon_2 z\exp\left(\frac{2\sqrt{2}\sigma_Y s_k + 2\mu_Y}{\xi}\right)\right]. \tag{66}$$

Substituting (65) and (66) into (63) yields the average capacity for node $\mathcal{A}$. However, the integral in (63) is difficult to obtain in closed-form. We approximate $\mathbb{E}[C_A]$ by applying the Gauss-Laguerre quadrature [59] as

$$\mathbb{E}[C_A] \approx \frac{1}{2\ln(2)}\sum_{j=0}^{1}\sum_{m=1}^{M} p_j \frac{\varrho_m}{\iota_m}\left(1 - \mathcal{M}_{\mathcal{Y}}(\delta_{m_j})\right)\mathcal{M}_{\mathcal{X}_j}(\delta_{m_j}), \tag{67}$$

where $\delta_{m_j} = \iota_m/\eta_j$, ϱ_m, and ι_m denote the weights and zeros of the M-order Laguerre polynomial, respectively, tabulated in [55, Table 25.9].

From (8), we have

$$\gamma_{Bj} = \frac{\mathcal{K}}{\mathcal{Z}_j + \omega_j}, \tag{68}$$

where $\mathcal{K} = \vartheta_1\vartheta_2 X$, $\vartheta_1 = P_A a_{AR}^2$, $\vartheta_2 = \beta^2 a_{RB}^2$, $\mathcal{Z}_j = \sigma_{Bj}^2 Y^{-1}$, and $\omega_j = \vartheta_2\sigma_{Rj}^2$. Following a similar analysis, the average capacity at node $\mathcal{B}$, $\mathbb{E}[C_B]$, is expressed as

$$\mathbb{E}[C_B] = \frac{1}{2\ln(2)}\sum_{j=0}^{1} p_j \int_0^\infty \frac{1}{z}(1 - \mathcal{M}_{\mathcal{K}}(z))e^{(-\omega_j z)}\mathcal{M}_{\mathcal{Z}_j}(z)dz, \tag{69}$$

where

$$\mathcal{M}_{\mathcal{K}}(z) \simeq \sum_{k=1}^{K} \frac{w_k}{\sqrt{\pi}} \times \exp\left[-\vartheta_1\vartheta_2 z\exp\left(\frac{2\sqrt{2}\sigma_X s_k + 2\mu_X}{\xi}\right)\right], \tag{70}$$

and

$$\mathcal{M}_{\mathcal{Z}_j}(z) \simeq \sum_{k=1}^{K} \frac{w_k}{\sqrt{\pi}} \times \exp\left[-\sigma_{Bj}^2 z \exp\left(-\frac{2\sqrt{2}\sigma_Y s_k + 2\mu_Y}{\xi}\right)\right]. \quad (71)$$

$\mathbb{E}[C_B]$ can also be approximated using the Gauss-Laguerre quadrature as

$$\mathbb{E}[C_B] \approx \frac{1}{2\ln(2)} \sum_{j=0}^{1} \sum_{m=1}^{M} p_j \frac{\varrho_m}{\iota_m} \left(1 - \mathcal{M}_{\mathcal{K}}(\varepsilon_{m_j})\right) \mathcal{M}_{\mathcal{Z}_j}(\varepsilon_{m_j}), \quad (72)$$

where $\varepsilon_{m_j} = \iota_m/\omega_j$, ϱ_m and ι_m denote the weights and zeros of the M-order Laguerre polynomial, respectively, tabulated in [55, Table 25.9]. This completes the proof.

APPENDIX B
PROOF OF THEOREM 2

To derive the average capacity at node $\mathcal{A}$, we first rewrite (20) as

$$C_A = \frac{1}{2} \sum_{j=0}^{1} p_j \log_2(1 + \min\left(\gamma_{BR_j}, \gamma_{RA_j}\right). \quad (73)$$

Now letting $\Upsilon_j = \min\left(\gamma_{BR_j}, \gamma_{RA_j}\right)$, the average capacity, $\mathbb{E}[C_A]$, is calculated as

$$\mathbb{E}[C_A] = \frac{1}{2\ln(2)} \sum_{j=0}^{1} p_j \int_0^{\infty} \ln(1+z) f_{\Upsilon_j}(z) dz. \quad (74)$$

When γ_{BR_j} and γ_{RA_j} are considered to be independent, the PDF of Υ_j is expressed as

$$f_{\Upsilon_j}(z) = f_{\gamma_{BR_j}}(z)\bar{F}_{\gamma_{RA_j}}(z) + f_{\gamma_{RA_j}}(z)\bar{F}_{\gamma_{BR_j}}(z). \quad (75)$$

From here, we have

$$\mathbb{E}[C_A] = \underbrace{\frac{1}{2\ln(2)} \sum_{j=0}^{1} p_j \int_0^{\infty} \ln(1+z) f_{\gamma_{BR_j}}(z)\bar{F}_{\gamma_{RA_j}}(z) dz}_{C_1} + \underbrace{\frac{1}{2\ln(2)} \sum_{j=0}^{1} p_j \int_0^{\infty} \ln(1+z) f_{\gamma_{RA_j}}(z)\bar{F}_{\gamma_{BR_j}}(z) dz}_{C_2}, \quad (76)$$

where

$$f_{\gamma_{BR_j}}(z) = \frac{\xi}{z\sqrt{2\pi\sigma_{\gamma_{BR}}^2}} \exp\left(-\frac{(\xi\ln(z) - \mu_{\gamma_{BR_j}})^2}{2\sigma_{\gamma_{BR}}^2}\right), \quad (77)$$

$$f_{\gamma_{RA_j}}(z) = \frac{\xi}{z\sqrt{2\pi\sigma_{\gamma_{RA}}^2}} \exp\left(-\frac{(\xi\ln(z) - \mu_{\gamma_{RA_j}})^2}{2\sigma_{\gamma_{RA}}^2}\right), \quad (78)$$

$$\bar{F}_{\gamma_{BR_j}}(z) = Q\left(\frac{\xi\ln(z) - \mu_{\gamma_{BR_j}}}{\sigma_{\gamma_{BR}}}\right), \quad (79)$$

and

$$\bar{F}_{\gamma_{RA_j}}(z) = Q\left(\frac{\xi\ln(z) - \mu_{\gamma_{RA_j}}}{\sigma_{\gamma_{RA}}}\right). \quad (80)$$

Using the log-normal distribution properties, the RVs are distributed as $\gamma_{BR_j} \sim \mathcal{N}(2\mu_Y + \xi\ln(P_B a_{BR}^2/\sigma_{R_j}^2), 4\sigma_Y^2)$, and $\gamma_{RA_j} \sim \mathcal{N}(2\mu_X + \xi\ln(P_R a_{RA}^2/\sigma_{A_j}^2), 4\sigma_X^2)$, respectively.

The integral in (76) is difficult to solve. Therefore, we utilize the approximation proposed in [60], [61] to evaluate $\mathbb{E}[C_A]$. From [61, eq. (4)], C_1 and C_2 are calculated as

$$C_1 \approx \frac{1}{2\ln(2)} \sum_{j=0}^{1} p_j \frac{2}{3} \Phi_{1_j}\left(\mu_{\gamma_{BR_j}}\right) + \frac{1}{6}\Phi_{1_j}\left(\mu_{\gamma_{BR_j}} + \sqrt{3}\sigma_{\gamma_{BR}}\right) + \frac{1}{6}\Phi_{1_j}\left(\mu_{\gamma_{BR_j}} - \sqrt{3}\sigma_{\gamma_{BR}}\right), \quad (81)$$

$$C_2 \approx \frac{1}{2\ln(2)} \sum_{j=0}^{1} p_j \frac{2}{3} \Phi_{2_j}\left(\mu_{\gamma_{RA_j}}\right) + \frac{1}{6}\Phi_{2_j}\left(\mu_{\gamma_{RA_j}} + \sqrt{3}\sigma_{\gamma_{RA}}\right) + \frac{1}{6}\Phi_{2_j}\left(\mu_{\gamma_{RA_j}} - \sqrt{3}\sigma_{\gamma_{RA}}\right), \quad (82)$$

where

$$\Phi_{1_j}(x) = \ln\left(1 + \exp\left(\frac{x}{\xi}\right)\right) Q\left(\frac{x - \mu_{\gamma_{RA_j}}}{\sigma_{\gamma_{RA}}}\right), \quad (83)$$

and

$$\Phi_{2_j}(x) = \ln\left(1 + \exp\left(\frac{x}{\xi}\right)\right) Q\left(\frac{x - \mu_{\gamma_{BR_j}}}{\sigma_{\gamma_{BR}}}\right). \quad (84)$$

By combining (81) and (82), we arrive at $\mathbb{E}[C_A]$ shown in (24). By following a similar procedure, the average capacity at node $\mathcal{B}$ is derived as (25).

The next step is to calculate the average multiple access capacity at the relay $\mathcal{R}$. The average capacity, $\mathbb{E}[C_{MAC}]$, is represented as

$$\mathbb{E}[C_{MAC}] = \frac{1}{2\ln(2)} \sum_{j=0}^{1} p_j \int_0^{\infty} \ln(1+z) f_{\chi_j} dz, \quad (85)$$

where the PDF f_{χ_j} represents the PDF of the sum of two log-normal RVs. The Fenton-Wilkinson approximation is used to compute the parameters of the approximated log-normal RV [53], [54]. Following a procedure similar to the one used in [54], the mean μ_{χ_j} and variance $\sigma_{\chi_j}^2$ are computed as (86) and (87) found, as shown at the bottom of the next page, where $\tau_{AR_j} = P_A a_{AR}^2/\sigma_{R_j}^2$ and $\tau_{BR_j} = P_B a_{BR}^2/\sigma_{R_j}^2$. The PDF f_{χ_j} is therefore expressed as

$$f_{\chi_j}(z) = \frac{\xi}{z\sqrt{8\pi\sigma_{\chi_j}^2}} \exp\left(-\frac{(\xi\ln(z) - 2\mu_{\chi_j})^2}{8\sigma_{\chi_j}^2}\right), \quad (88)$$

By letting $t = \left(\xi \ln(z) - 2\mu_{\chi_j}\right) / \left(\sqrt{8\sigma_{\chi_j}^2}\right)$, (85) is rewritten as

$$\mathbb{E}[C_{MAC}] = \frac{1}{2\ln(2)} \sum_{j=0}^{1} p_j \int_{-\infty}^{\infty} \frac{H(t)}{\sqrt{\pi}} \exp(-t^2) dt, \quad (89)$$

where

$$H(t) = \ln\left(1 + \exp\left(\frac{\sqrt{8\sigma_{\chi_j}^2}\, t + 2\mu_{\chi_j}}{\xi}\right)\right). \quad (90)$$

From here, the average capacity of the MAC phase is attained in (23) using the Gauss-Hermite quadrature where w_k and s_k denote the weights and zeros of the K-order Hermite polynomial, respectively tabulated in [55, Table 25.10]. This completes the proof.

APPENDIX C
PROOF OF THEOREM 3

For the PLC AF TWR, the outage probability is written as [57]

$$P_{out_j}^{AF} = \underbrace{\Pr(\gamma_{A_j} < \gamma_{th})}_{I_{A_j}} + \underbrace{\Pr(\gamma_{B_j} < \gamma_{th})}_{I_{B_j}} - \underbrace{\Pr(\gamma_{A_j} < \gamma_{th}, \gamma_{B_j} < \gamma_{th})}_{I_{AB_j}}. \quad (91)$$

From (91), we have

$$\begin{aligned} I_{A_j} &= \Pr\left(\frac{\mathcal{Y}}{\mathcal{X}_j + \eta_j} < \gamma_{th}\right) \\ &= \Pr\left(\mathcal{Y} < \gamma_{th}\left(\mathcal{X}_j + \eta_j\right)\right) \end{aligned} \quad (92)$$

Conditioning on $\mathcal{X}_j$, I_{A_j} is further expressed as

$$\begin{aligned} I_{A_j} &= 1 - \Pr\left(\mathcal{Y} > \gamma_{th}\left(\mathcal{X}_j + \eta_j\right) | \mathcal{X}_j = z\right) \\ &= 1 - \int_0^{\infty} \bar{F}_{\mathcal{Y}}\left(\gamma_{th}(z + \eta_j)\right) f_{\mathcal{X}_j}(z) dz \end{aligned} \quad (93)$$

where

$$\bar{F}_{\mathcal{Y}}\left(\gamma_{th}(z + \eta_j)\right) = Q\left(\frac{\xi \ln(\gamma_{th}(z + \eta_j)) - \mu_{\mathcal{Y}}}{\sigma_{\mathcal{Y}}}\right), \quad (94)$$

and

$$f_{\mathcal{X}_j}(z) = \frac{\xi}{z\sqrt{2\pi\sigma_{\mathcal{X}}^2}} \exp\left(-\frac{(\xi \ln(z) - \mu_{\mathcal{X}_j})^2}{2\sigma_{\mathcal{X}}^2}\right). \quad (95)$$

The RVs $\mathcal{Y}$ and $\mathcal{X}_j$ are distributed as $\mathcal{Y} \sim \mathcal{N}(2\mu_Y + \xi \ln(\epsilon_1\epsilon_2), 4\sigma_Y^2)$, and $\mathcal{X}_j \sim \mathcal{N}(-2\mu_X + \xi \ln(\sigma_{A_j}^2), 4\sigma_X^2)$, respectively. By using the approximation in [61, eq. (4)], we evaluate I_{A_j} as (31). The outage probability at node $\mathcal{B}$, I_{B_j} can be found in a similar manner using (32) where the RVs $\mathcal{K}$ and $\mathcal{Z}_j$ are distributed as $\mathcal{K} \sim \mathcal{N}(2\mu_X + \xi \ln(\vartheta_1\vartheta_2), 4\sigma_X^2)$, and $\mathcal{Z}_j \sim \mathcal{N}(-2\mu_Y + \xi \ln(\sigma_{B_j}^2), 4\sigma_Y^2)$, respectively.

The next step is to calculate the outage probability, I_{AB_j}. In order to derive I_{AB_j}, the outage probability is expanded as

$$\Pr\left(Y < \frac{\sigma_{R_j}^2\gamma_{th}}{\epsilon_1} + \frac{\sigma_{A_j}^2\gamma_{th}}{\epsilon_1\epsilon_2 X}, X < \frac{\sigma_{R_j}^2\gamma_{th}}{\vartheta_1} + \frac{\sigma_{B_j}^2\gamma_{th}}{\vartheta_1\vartheta_2 X}\right). \quad (96)$$

From here, we have

$$\begin{aligned} I_{AB_j} = &\underbrace{\int_0^{\Lambda_{X_j}} \int_{\frac{\Lambda_{Y_j}}{\Lambda_{X_j}}x}^{\frac{\gamma_{th}}{\epsilon_1}\left(\sigma_{R_j}^2 + \frac{\sigma_{A_j}^2}{\epsilon_2 x}\right)} f_X(x) f_Y(y) dy dx}_{I_{1_j}} \\ &+ \underbrace{\int_0^{\Lambda_{Y_j}} \int_{\frac{\Lambda_{X_j}}{\Lambda_{Y_j}}y}^{\frac{\gamma_{th}}{\vartheta_1}\left(\sigma_{R_j}^2 + \frac{\sigma_{B_j}^2}{\vartheta_2 y}\right)} f_X(x) f_Y(y) dx dy}_{I_{2_j}}, \end{aligned} \quad (97)$$

where

$$I_{1_j} = \int_0^{\Lambda_{X_j}} f_X(x) \left[F_Y\left(\frac{\gamma_{th}}{\epsilon_1}\left(\sigma_{R_j}^2 + \frac{\sigma_{A_j}^2}{\epsilon_2 x}\right)\right) - F_Y\left(\frac{\Lambda_{Y_j}}{\Lambda_{X_j}}x\right)\right] dx, \quad (98)$$

$$\mu_{\chi_j} = \frac{\xi}{2}\left(\ln\left[\sum_{m\in\{AR,BR\}} \exp(2\xi^{-1}\mu_m + \ln\left(\tau_{m_j}\right) + 2\xi^{-2}\sigma_m^2)\right] - 2\xi^{-2}\sigma_{\chi_j}^2\right), \quad (86)$$

$$\sigma_{\chi_j}^2 = \frac{\xi^2}{4} \ln\left[\frac{\sum_{m\in\{AR,BR\}} \exp(4\xi^{-1}\mu_m + 2\ln\left(\tau_{m_j}\right) + 8\xi^{-2}\sigma_m^2) - \sum_{m\in\{AR,BR\}} \exp(4\xi^{-1}\mu_m + 2\ln\left(\tau_{m_j}\right) + 4\xi^{-2}\sigma_m^2)}{\left(\sum_{m\in\{AR,BR\}} \exp\left(2\xi^{-1}\mu_m + \ln\left(\tau_{m_j}\right) + 2\xi^{-2}\sigma_m^2\right)\right)^2} + 1\right]. \quad (87)$$

and

$$I_{2_j}=\int_0^{\Lambda_{Y_j}} f_Y(y)\left[F_X\left(\frac{\gamma_{th}}{\vartheta_1}\left(\sigma_{R_j}^2+\frac{\sigma_{B_j}^2}{\vartheta_{2y}}\right)\right)-F_X\left(\frac{\Lambda_{X_j}}{\Lambda_{Y_j}}y\right)\right]dy. \tag{99}$$

$(\Lambda_{X_j}, \Lambda_{Y_j})$ is a solution of the following equations [57]

$$\begin{cases} x=\dfrac{\gamma_{th}}{\vartheta_1}\left(\sigma_{R_j}^2+\dfrac{\sigma_{B_j}^2}{\vartheta_{2y}}\right), \\ y=\dfrac{\gamma_{th}}{\epsilon_1}\left(\sigma_{R_j}^2+\dfrac{\sigma_{A_j}^2}{\epsilon_2 x}\right). \end{cases} \tag{100}$$

After solving (100), the solution points $(\Lambda_{X_j}, \Lambda_{Y_j})$ are given, respectively, as

$$\Lambda_{X_j}=\frac{\phi_1+\sqrt{\phi_1^2+4\epsilon_2\sigma_{A_j}^2(\sigma_{R_j}^2)^2\vartheta_1\vartheta_2^2\gamma_{th}}}{2\epsilon_2\sigma_{R_j}^2\vartheta_1\vartheta_2}, \tag{101}$$

and

$$\Lambda_{Y_j}=\frac{\phi_2+\sqrt{\phi_1^2+4\epsilon_2\sigma_{A_j}^2(\sigma_{R_j}^2)^2\vartheta_1\vartheta_2^2\gamma_{th}}}{2\epsilon_1\epsilon_2\sigma_{R_j}^2\vartheta_2} \tag{102}$$

where $\phi_1=\epsilon_1\epsilon_2\sigma_{B_j}^2-\sigma_{A_j}^2\vartheta_1\vartheta_2+\epsilon_2(\sigma_{R_j}^2)^2\vartheta_2\gamma_{th}$ and $\phi_2=-\epsilon_1\epsilon_2\sigma_{B_j}^2+\sigma_{A_j}^2\vartheta_1\vartheta_2+\epsilon_2(\sigma_{R_j}^2)^2\vartheta_2\gamma_{th}$. From here, I_{1_j} and I_{2_j} are rewritten, respectively, as

$$I_{1_j}=\int_0^{\Lambda_{X_j}}\left[F_Y\left(\Psi_{3_j}\right)-F_Y\left(\Psi_{4_j}\right)\right]f_X(x)dx, \tag{103}$$

and

$$I_{2_j}=\int_0^{\Lambda_{Y_j}}\left[F_X\left(\Psi_{5_j}\right)-F_X\left(\Psi_{6_j}\right)\right]f_Y(y)dy, \tag{104}$$

where

$$F_Y\left(\Psi_{3_j}\right)=1-Q\left(\frac{\xi\ln(\Psi_{3_j})-2\mu_Y}{2\sigma_Y}\right), \tag{105}$$

$$F_Y\left(\Psi_{4_j}\right)=1-Q\left(\frac{\xi\ln(\Psi_{4_j})-2\mu_Y}{2\sigma_Y}\right), \tag{106}$$

$$F_X\left(\Psi_{5_j}\right)=1-Q\left(\frac{\xi\ln(\Psi_{5_j})-2\mu_X}{2\sigma_X}\right), \tag{107}$$

$$F_X\left(\Psi_{6_j}\right)=1-Q\left(\frac{\xi\ln(\Psi_{6_j})-2\mu_X}{2\sigma_X}\right), \tag{108}$$

$$f_X(x)=\frac{\xi}{x\sqrt{8\pi\sigma_X^2}}\exp\left(-\frac{(\xi\ln(x)-2\mu_X)^2}{8\sigma_X^2}\right), \tag{109}$$

$$f_Y(y)=\frac{\xi}{y\sqrt{8\pi\sigma_Y^2}}\exp\left(-\frac{(\xi\ln(y)-2\mu_Y)^2}{8\sigma_Y^2}\right), \tag{110}$$

and

$$\Psi_{3_j}=\frac{\gamma_{th}}{\epsilon_1}\left(\sigma_{R_j}^2+\frac{\sigma_{A_j}^2}{\epsilon_2 x}\right), \Psi_{4_j}=\frac{\Lambda_{Y_j}}{\Lambda_{X_j}}x,$$
$$\Psi_{5_j}=\frac{\gamma_{th}}{\vartheta_1}\left(\sigma_{R_j}^2+\frac{\sigma_{B_j}^2}{\vartheta_{2y}}\right), \Psi_{6_j}=\frac{\Lambda_{X_j}}{\Lambda_{Y_j}}y. \tag{111}$$

I_{1_j} and I_{2_j} can be further expressed as (112), and (113) as shown at bottom of this page. Using [61, eq. (4)] and

$$I_{1_j}=\underbrace{\int_0^{\Lambda_{X_j}}\frac{\xi}{x\sqrt{8\pi\sigma_X^2}}\exp\left(-\frac{(\xi\ln(x)-2\mu_X)^2}{8\sigma_X^2}\right)Q\left(\frac{\xi\ln(\Psi_{4_j})-2\mu_Y}{2\sigma_Y}\right)dx}_{J_{1j}}$$
$$-\underbrace{\int_0^{\Lambda_{X_j}}\frac{\xi}{x\sqrt{8\pi\sigma_X^2}}\exp\left(-\frac{(\xi\ln(x)-2\mu_X)^2}{8\sigma_X^2}\right)Q\left(\frac{\xi\ln(\Psi_{3_j})-2\mu_Y}{2\sigma_Y}\right)dx}_{J_{2j}}, \tag{112}$$

$$I_{2_j}=\underbrace{\int_0^{\Lambda_{Y_j}}\frac{\xi}{y\sqrt{8\pi\sigma_Y^2}}\exp\left(-\frac{(\xi\ln(y)-2\mu_Y)^2}{8\sigma_Y^2}\right)Q\left(\frac{\xi\ln(\Psi_{6_j})-2\mu_X}{2\sigma_X}\right)dy}_{J_{3j}}$$
$$-\underbrace{\int_0^{\Lambda_{Y_j}}\frac{\xi}{y\sqrt{2\pi\sigma_Y^2}}\exp\left(-\frac{(\xi\ln(y)-2\mu_Y)^2}{8\sigma_Y^2}\right)Q\left(\frac{\xi\ln(\Psi_{5_j})-2\mu_X}{2\sigma_X}\right)dy}_{J_{4j}}, \tag{113}$$

[62, eq. (15)], I_{1_j} and I_{2_j} are expressed as (35) and (37), respectively.

Finally, by combining (31), (32), (35), and (37), the outage probability for the PLC AF TWR is found. This completes the proof.

APPENDIX D
PROOF OF THEOREM 4

We derive the outage probability of the PLC DF TWR with PNC in (42). For simplicity, we only consider the high rate case where $\gamma_{th} \geq 1$ [18]. The outage probability of the PLC DF TWR with PNC is expressed as

$$P_{out}^{DF,PNC} = \sum_{j=0}^{1} p_j P_{out_j}^{DF,PNC}, \tag{114}$$

From (41), we have

$$P_{out_j}^{DF,PNC} = 1 - \int_{\frac{\sigma_{B_j}^2 \gamma_{th}}{P_R a_{RB}^2}}^{\infty} \int_{\frac{\gamma_{th}(P_B a_{BR}^2 y + \sigma_{R_j}^2)}{P_A a_{AR}^2}}^{\infty} f_X(x) f_Y(y) dx dy - \int_{\frac{\sigma_{A_j}^2 \gamma_{th}}{P_R a_{RA}^2}}^{\infty} \int_{\frac{\gamma_{th}(P_A a_{AR}^2 x + \sigma_{R_j}^2)}{P_B a_{BR}^2}}^{\infty} f_X(x) f_Y(y) dx dy. \tag{115}$$

Finally, the outage probability of the PLC DF TWR with PNC is

$$P_{out_j}^{DF,PNC} = 1 - \int_{\frac{\sigma_{B_j}^2 \gamma_{th}}{P_R a_{RB}^2}}^{\infty} f_X(y) Q\left(\frac{\xi \ln(\Gamma_j) - 2\mu_Y}{2\sigma_Y}\right) dy - \int_{\frac{\sigma_{A_j}^2 \gamma_{th}}{P_R a_{RA}^2}}^{\infty} f_Y(x) Q\left(\frac{\xi \ln(\Xi_j) - 2\mu_X}{2\sigma_X}\right) dx, \tag{116}$$

where

$$\Gamma_j = \frac{\gamma_{th}\left(P_B a_{BR}^2 y + \sigma_{R_j}^2\right)}{P_A a_{AR}^2}, \tag{117}$$

and

$$\Xi_j = \frac{\gamma_{th}\left(P_A a_{AR}^2 x + \sigma_{R_j}^2\right)}{P_B a_{BR}^2}. \tag{118}$$

The PDFs $f_X(y)$ and $f_Y(x)$ are determined using (109) and (110), respectively. By substituting $f_X(y)$ and $f_Y(x)$ into (116), we get (42). This completes the proof.

REFERENCES

[1] S. Galli, A. Scaglione, and Z. Wang, "For the grid and through the grid: The role of power line communications in the smart grid," *Proc. IEEE*, vol. 99, no. 6, pp. 998–1027, Jun. 2011.
[2] L. T. Berger, A. Schwager, P. Pagani, and D. M. Schneider, "MIMO power line communications," *IEEE Commun. Surveys Tuts.*, vol. 17, no. 1, pp. 106–124, 1st Quart., 2015.
[3] Y. Ben-Yehezkel, R. Gazit, and A. Haidine, "Performance evaluation of medium access control mechanisms in high-speed narrowband PLC for smart grid applications," in *Proc. IEEE Int. Symp. Power Line Commun. Appl.*, Mar. 2012, pp. 94–101.
[4] *IEEE Standard for Broadband over Power Line Networks: Medium Access Control and Physical Layer Specifications*, IEEE Commun. Society Standard 1901-2010, Dec. 2010.
[5] *HomePlug Green PHY Specification Release Version 1.1*, HomePlug Alliance Standard, Jan. 2012. [Online]. Available: http://www.homeplug.org/tech/whitepapers/HomePlug_Green_PHY_whitepaper_121003.pdf
[6] D. Schneider, J. Speidel, L. Stadelmeier, and D. Schill, "Precoded spatial multiplexing MIMO for inhome power line communications," in *Proc. IEEE Global Telecommun. Conf. (GLOBECOM)*, Nov. 2008, pp. 1–5.
[7] K. M. Rabie, B. Adebisi, E. H. G. Yousif, H. Gacanin, and A. M. Tonello, "A comparison between orthogonal and non-orthogonal multiple access in cooperative relaying power line communication systems," *IEEE Access*, vol. 5, pp. 10118–10129, 2017.
[8] M. S. P. Facina, H. A. Latchman, H. V. Poor, and M. V. Ribeiro, "Cooperative in-home power line communication: Analyses based on a measurement campaign," *IEEE Trans. Commun.*, vol. 64, no. 2, pp. 778–789, Feb. 2016.
[9] X. Cheng, R. Cao, and L. Yang, "Relay-aided amplify-and-forward power-line communications," *IEEE Trans. Smart Grid*, vol. 4, no. 1, pp. 265–272, Mar. 2013.
[10] J.-H. Lee and Y.-H. Kim, "Diversity relaying for parallel use of power-line and wireless communication networks," *IEEE Trans. Power Del.*, vol. 29, no. 3, pp. 1301–1310, Jun. 2014.
[11] Leonardo de M. B. A. Dib, V. Fernandes, Mateus de L. Filomeno, and M. V. Ribeiro, "Hybrid PLC/wireless communication for smart grids and Internet of Things applications," *IEEE Internet Things J.*, vol. 5, no. 2, pp. 655–667, Apr. 2018.
[12] V. Fernandes, H. V. Poor, and M. V. Ribeiro, "A hybrid power line/wireless dual-hop system with energy harvesting relay," *IEEE Internet Things J.*, vol. 5, no. 5, pp. 4201–4211, Oct. 2018.
[13] A. El Shafie, M. F. Marzban, R. Chabaan, and N. Al-Dhahir, "An artificial-noise-aided secure scheme for hybrid parallel PLC/wireless OFDM systems," in *Proc. IEEE Int. Conf. Commun.*, May 2018, pp. 1–6.
[14] Y. Qian, J. Yan, H. Guan, J. Li, X. Zhou, S. Guo, and D. N. K. Jayakody, "Design of hybrid wireless and power line sensor networks with dual-interface relay in IoT," *IEEE Internet Things J.*, vol. 6, no. 1, pp. 239–249, Feb. 2019.
[15] K. Azarian, H. El Gamal, and P. Schniter, "On the achievable diversity-multiplexing tradeoff in half-duplex cooperative channels," *IEEE Trans. Inf. Theory*, vol. 51, no. 12, pp. 4152–4172, Dec. 2005.
[16] B. Rankov and A. Wittneben, "Spectral efficient protocols for half-duplex fading relay channels," *IEEE J. Sel. Areas Commun.*, vol. 25, no. 2, pp. 379–389, Feb. 2007.
[17] R. H. Y. Louie, Y. Li, and B. Vucetic, "Practical physical layer network coding for two-way relay channels: Performance analysis and comparison," *IEEE Trans. Wireless Commun.*, vol. 9, no. 2, pp. 764–777, Feb. 2010.
[18] Z. Zhang, Z. Ma, Z. Ding, M. Xiao, and G. K. Karagiannidis, "Full-duplex two-way and one-way relaying: Average rate, outage probability, and tradeoffs," *IEEE Trans. Wireless Commun.*, vol. 15, no. 6, pp. 3920–3933, Jun. 2016.
[19] K.-J. Lee, H. Sung, E. Park, and I. Lee, "Joint optimization for one and two-way MIMO AF multiple-relay systems," *IEEE Trans. Wireless Commun.*, vol. 9, no. 12, pp. 3671–3681, Dec. 2010.
[20] K.-J. Lee, K. W. Lee, H. Sung, and I. Lee, "Sum-rate maximization for two-way MIMO amplify-and-forward relaying systems," in *Proc. IEEE Veh. Technol. Conf.*, Apr. 2009, pp. 1–5.
[21] K.-J. Lee and I. Lee, "Achievable rate regions for two-way MIMO AF multiple-relay channels," in *Proc. IEEE Veh. Technol. Conf.*, May 2011, pp. 1–5.
[22] C. Xu, Z. Li, L. Zhong, H. Zhang, and G. M. Muntean, "CMT-NC: Improving the concurrent multipath transfer performance using network coding in wireless networks," *IEEE Trans. Veh. Technol.*, vol. 65, no. 3, pp. 1735–1751, Mar. 2016.
[23] N. Khyaria, S. Khalfallahb, Y. Barounib, and J. B. H. Slama, "Decode and forward relay-assisted power-line communication," *Procedia Comput. Sci.*, vol. 73, pp. 209–216, Dec. 2015.

[24] G. Levin and S. Loyka, "Amplify-and-forward versus decode-and-forward relaying: Which is better?" in *Proc. Int. Zürich Semin. Commun.*, Mar. 2012, pp. 236–241.
[25] C. Song, K.-J. Lee, and I. Lee, "Performance analysis of MMSE-based amplify and forward spatial multiplexing MIMO relaying systems," *IEEE Trans. Commun.*, vol. 59, no. 12, pp. 3452–3462, Dec. 2011.
[26] C. Song, K.-J. Lee, and I. Lee, "MMSE-based MIMO cooperative relaying systems: Closed-form designs and outage behavior," *IEEE J. Sel. Areas Commun.*, vol. 30, no. 8, pp. 1390–1401, Sep. 2012.
[27] C. Song, K.-J. Lee, and I. Lee, "MMSE based transceiver designs in closed-loop non-regenerative MIMO relaying systems," *IEEE Trans. Wireless Commun.*, vol. 9, no. 7, pp. 2310–2319, Jul. 2010.
[28] K.-J. Lee, J.-S. Kim, G. Caire, and I. Lee, "Asymptotic ergodic capacity analysis for MIMO amplify-and-forward relay networks," *IEEE Trans. Wireless Commun.*, vol. 9, no. 9, pp. 2712–2717, Sep. 2010.
[29] K. M. Rabie and B. Adebisi, "Enhanced amplify-and-forward relaying in non-Gaussian PLC networks," *IEEE Access*, vol. 5, pp. 4087–4094, 2017.
[30] K. M. Rabie, B. Adebisi, A. M. Tonello, and G. Nauryzbayev, "For more energy-efficient dual-hop DF relaying power-line communication systems," *IEEE Syst. J.*, vol. 12, no. 2, pp. 2005–2016, Jun. 2018.
[31] F. Passerini and A. M. Tonello, "Analog full-duplex amplify-and-forward relay for power line communication networks," *IEEE Commun. Lett.*, vol. 23, no. 4, pp. 676–679, Apr. 2019.
[32] N. Agrawal, P. K. Sharma, and T. A. Tsiftsis, "Multihop DF relaying in NB-PLC system over Rayleigh fading and Bernoulli–Laplacian noise," *IEEE Syst. J.*, vol. 13, no. 1, pp. 357–364, Mar. 2019.
[33] A. Dubey, C. Kundu, T. M. N. Ngatched, O. A. Dobre, and R. K. Mallik, "Incremental relaying for power line communications: Performance analysis and power allocation," *IEEE Syst. J.*, to be published. doi: 10.1109/JSYST.2018.2879162.
[34] Y.-W. Qian, M. Tian, X. Jian, H.-J. Song, S. Feng, and J. Li, "Performance analysis for a two-way relaying power line network with analog network coding," *Frontiers Inf. Technol. Electron. Eng.*, vol. 16, no. 10, pp. 892–898, Oct. 2015. doi: 10.1631/FITEE.1500135.
[35] B. Tan and J. Thompson, "Relay transmission protocols for in-door powerline communications networks," in *Proc. IEEE Int. Conf. Commun. Workshops*, Jun. 2011, pp. 1–5.
[36] X. Wu and Y. Rong, "Joint terminals and relay optimization for two-way power line information exchange systems with QoS constraints," *EURASIP J. Adv. Signal Process.*, vol. 2015, no. 84, pp. 1–15, Sep. 2015.
[37] Q. Yang, H. Wang, T. Wang, L. You, L. Lu, and S. C. Liew, "Powerline-PNC: Boosting throughput of powerline networks with physical-layer network coding," in *Proc. IEEE Int. Conf. Smart Grid Commun.*, Nov. 2015, pp. 103–108.
[38] F. Versolatto and A. M. Tonello, "Analysis of the PLC channel statistics using a bottom-up random simulator," in *Proc. IEEE Int. Symp. Power Line Commun. Appl.*, Mar. 2010, pp. 123–126.
[39] S. Galli, "A novel approach to the statistical modeling of wireline channels," *IEEE Trans. Commun.*, vol. 59, no. 5, pp. 1332–1345, May 2011.
[40] A. M. Tonello, F. Versolatto, and A. Pittolo, "In-home power line communication channel: Statistical characterization," *IEEE Trans. Commun.*, vol. 62, no. 6, pp. 2096–2106, Jun. 2014.
[41] C. Cano, A. Pittolo, D. Malone, L. Lampe, A. M. Tonello, and A. G. Dabak, "State of the art in power line communications: From the applications to the medium," *IEEE J. Sel. Areas Commun.*, vol. 34, no. 7, pp. 1935–1952, Jul. 2016.
[42] M. De Piante and A. M. Tonello, "Characteristics of the PLC channel: Reciprocity, symmetry and port decoupling for impedance matching," in *Proc. IEEE Int. Symp. Power Line Commun. Appl.*, Mar. 2016, pp. 93–97.
[43] C. W. R. Chiong, Y. Rong, and Y. Xiang, "Channel training algorithms for two-way MIMO relay systems," *IEEE Trans. Signal Process.*, vol. 61, no. 16, pp. 3988–3998, Aug. 2013.
[44] F. Gao, R. Zhang, and Y.-C. Liang, "Optimal channel estimation and training design for two-way relay networks," *IEEE Trans. Commun.*, vol. 57, no. 10, pp. 3024–3033, Oct. 2009.
[45] Z. Jiang, H. Wang, and Z. Ding, "A Bayesian algorithm for joint symbol timing synchronization and channel estimation in two-way relay networks," *IEEE Trans. Commun.*, vol. 61, no. 10, pp. 4271–4283, Oct. 2013.
[46] Q. Li, S. H. Ting, A. Pandharipande, and Y. Han, "Adaptive two-way relaying and outage analysis," *IEEE Trans. Wireless Commun.*, vol. 8, no. 6, pp. 3288–3299, Jun. 2009.
[47] M. Zimmermann and K. Dostert, "A multipath model for the powerline channel," *IEEE Trans. Commun.*, vol. 50, no. 4, pp. 553–559, Apr. 2002.
[48] L. D. Bert, P. Caldera, D. Schwingshackl, and A. M. Tonello, "On noise modeling for power line communications," in *Proc. IEEE Int. Symp. Power Line Commun. Appl. (ISPLC)*, Apr. 2011, pp. 283–288.
[49] A. Salem, K. A. Hamdi, and E. Alsusa, "Physical layer security over correlated log-normal cooperative power line communication channels," *IEEE Access*, vol. 5, pp. 13909–13921, 2017.
[50] M. O. Hasna and M. S. Alouini, "A performance study of dual-hop transmissions with fixed gain relays," *IEEE Trans. Wireless Commun.*, vol. 3, no. 6, pp. 1963–1968, Nov. 2004.
[51] X. Liang, S. Jin, X. Gao, and K. K. Wong, "Outage performance for decode-and-forward two-way relay network with multiple interferers and noisy relay," *IEEE Trans. Commun.*, vol. 61, no. 2, pp. 521–531, Feb. 2013.
[52] C. Li, Z. Chen, Y. Wang, Y. Yao, and B. Xia, "Outage analysis of the full-duplex decode-and-forward two-way relay system," *IEEE Trans. Veh. Technol.*, vol. 66, no. 5, pp. 4073–4086, May 2017.
[53] N. B. Mehta, J. Wu, A. F. Molisch, and J. Zhang, "Approximating a sum of random variables with a lognormal," *IEEE Trans. Wireless Commun.*, vol. 6, no. 7, pp. 2690–2699, Jul. 2007.
[54] L. Fenton, "The sum of log-normal probability distributions in scatter transmission systems," *IRE Trans. Commun. Syst.*, vol. 8, no. 1, pp. 57–67, Mar. 1960.
[55] M. Abramowitz and I. Stegun, *Handbook of Mathematical Functions: With Formulas, Graphs, and Mathematical Tables*, 9th ed. New York, NY, USA: Dover, 1972.
[56] A. Dubey and R. K. Mallik, "PLC system performance with AF relaying," *IEEE Trans. Commun.*, vol. 63, no. 6, pp. 2337–2345, Jun. 2015.
[57] Z. Chen, B. Xia, and H. Liu, "Wireless information and power transfer in two-way amplify-and-forward relaying channels," in *Proc. IEEE GlobalSIP*, Atlanta, GA, USA, Dec. 2014, pp. 168–172.
[58] K. A. Hamdi, "A useful lemma for capacity analysis of fading interference channels," *IEEE Trans. Commun.*, vol. 58, no. 2, pp. 411–416, Feb. 2010.
[59] S. Zhou, X. Wang, N. Cao, and X. Li, "Performance analysis of wireless powered communications with multiple antennas," *IEEE Access*, vol. 6, pp. 15541–15549, 2018.
[60] J. M. Holtzman, "A simple, accurate method to calculate spread-spectrum multiple-access error probabilities," *IEEE Trans. Commun.*, vol. 40, no. 3, pp. 461–464, Mar. 1992.
[61] G. Pan, C. Tang, X. Zhang, T. Li, Y. Weng, and Y. Chen, "Physical-layer security over non-small-scale fading channels," *IEEE Trans. Veh. Technol.*, vol. 65, no. 3, pp. 1326–1339, Mar. 2016.
[62] L. Yang, K. Qaraqe, E. Serpedin, and X. Gao, "Performance analysis of two-way relaying networks with the Nth worst relay selection over various fading channels," *IEEE Trans. Veh. Technol.*, vol. 64, no. 7, pp. 3321–3327, Jul. 2015.

ROGER KWAO AHIADORMEY (S'17) received the B.Sc. degree in electrical/electronic engineering from the Kwame Nkrumah University of Science and Technology (KNUST), Ghana, in 2012, and the M.S. degree in electronic engineering from Hanbat National University, South Korea, in 2016, where he is currently pursuing the Ph.D. degree with the Department of Electronic Engineering. His research interests include physical-layer security, power line communication, and massive MIMO.

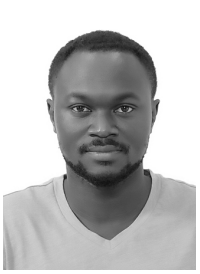

PRINCE ANOKYE (S15–M'19) received the B.Sc. degree in computer engineering and the M.Sc. degree in telecommunication engineering from the Kwame Nkrumah University of Science and Technology (KNUST), Ghana, in 2010 and 2014, respectively, and the Ph.D. degree in electronic engineering from Hanbat National University, South Korea, in 2019, where he is currently a Postdoctoral Research Fellow with the Department of Electronic and Control Engineering. His research interests include massive MIMO, full-duplex communication, and heterogeneous cellular networks.

HAN-SHIN JO (S'06–M'10) received the B.S., M.S., and Ph.D. degrees in electrical and electronics engineering from Yonsei University, Seoul, South Korea, in 2001, 2004, and 2009, respectively. He was a Postdoctoral Research Fellow with the Wireless Network and Communications Group, Department of Electrical and Computer Engineering, The University of Texas at Austin, from 2009 to 2011. He developed a long-term evolution base station in Samsung Electronics, from 2011 to 2012. He is currently an Associate Professor with the Department of Electronics and Control Engineering, Hanbat National University, Daejeon, South Korea. His current research interests include all the aspects of MIMO (channel modeling, precoding, and scheduling with limited feedback, beamforming, SDMA, and massive MIMO) and applications of stochastic geometry and optimization theory to wireless cellular and ad hoc networks.

Dr. Jo was a recipient of the Samsung Electronics Graduate Fellowship, from 2006 to 2008, the Korea Research Foundation BrainKorea21 Graduate Fellowship, from 2006 to 2007, the Korea Research Foundation Post-Doctoral Fellowship, in 2009, and the 2011 ETRI Journal Best Paper Award.

KYOUNG-JAE LEE (S'06–M'11) received the B.S., M.S., and Ph.D. degrees from the School of Electrical Engineering, Korea University, Seoul, South Korea, in 2005, 2007, and 2011, respectively. In 2006, he interned at Beceem Communications, Inc., Santa Clara, CA, USA, and in 2009, he visited the University of Southern California, Los Angeles, CA, USA, as a Visiting Student. He was a Research Professor with Korea University, in 2011. From 2011 to 2012, he was a Postdoctoral Fellow with the Wireless Networking and Communications Group, The University of Texas at Austin, Austin, TX, USA. Since 2012, he has been with the Department of Electronics and Control Engineering, Hanbat National University, Daejeon, South Korea, where he is currently an Associate Professor. His research interests include communication theory, signal processing, and information theory applied to the next-generation wireless communications. He was a recipient of the Best Paper Award at the IEEE VTC Fall, in 2009, the IEEE ComSoc APB Outstanding Paper Award, in 2013, and the IEEE ComSoc APB Outstanding Young Researcher, in 2013.